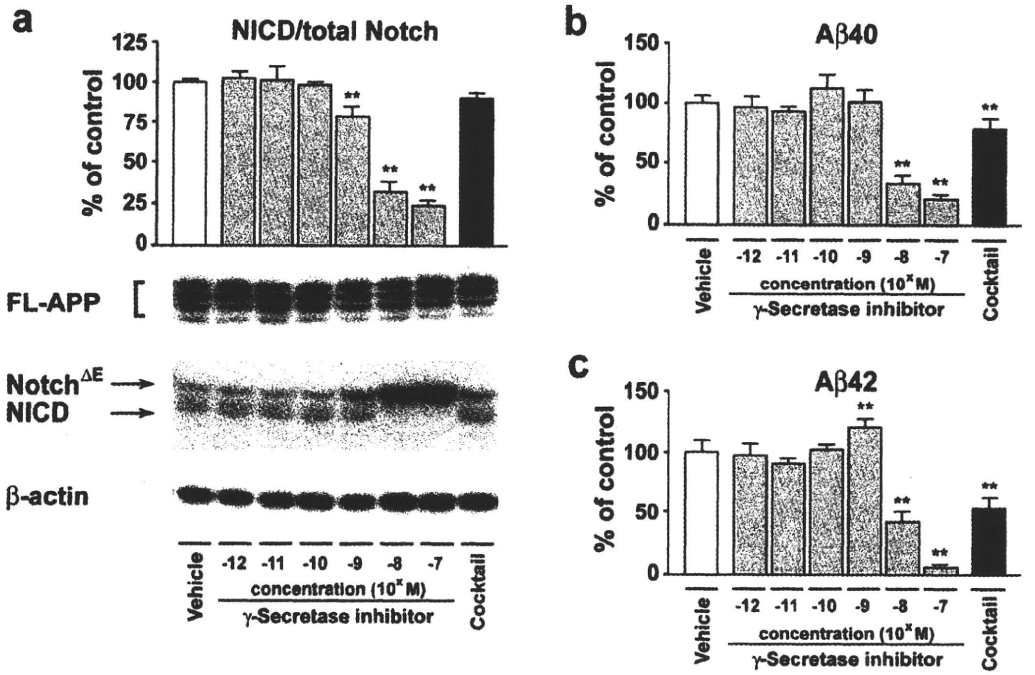

Fig. 5. Comparison between the γ-secretase inhibitor and four-drug cocktail in Notch processing and Aβ40 and Aβ42 levels. Amount of Notch fragments in the cell lysate of mNotch$^{\Delta E}$-N2a cells (**a**) or Aβ released into the conditioned medium from mNotch$^{\Delta E}$-N2a cells (**b,c**) treated with the γ-secretase inhibitor or four-drug cocktail was measured by semiquantitative Western blot analysis or sandwich ELISA, respectively. Data represent the mean ± SD of four experiments (a–c). Sample Western blots are shown for FL-APP, Notch$^{\Delta E}$, NICD, and β-actin (a). Levels of Aβ are expressed as Aβ40 (b) and Aβ42 (c). $^{**}P < 0.01$, significantly different from the vehicle-treated group (a–c). FL, full-length; NICD, Notch intracellular domain.

proteins other than APP as an adverse effect (De Strooper et al., 1999; Geling et al., 2002; Wong et al., 2004). To compare the effects of the four-drug cocktail with that of the γ-secretase inhibitor alone on Notch processing and Aβ production, we investigated the ratio of NICD (Notch intracellular domain) to total Notch and both Aβ40 and Aβ42 levels in the conditioned media from mNotch$^{\Delta E}$-N2a cells by semiquantitative Western blot analysis and sandwich ELISA, respectively (Fig. 5). Notch processing was significantly inhibited by the γ-secretase inhibitor at more than 10^{-9} M. However, the four-drug cocktail treatment had no significant effect on Notch processing (NICD/total Notch = 90.5% ± 3.6%; Fig. 5a) and significantly reduced both Aβ40 and Aβ42 levels (Aβ40 level = 78.8% ± 9.9%, Aβ42 level = 53.3% ± 8.2%) compared with the vehicle-treated group (Fig. 5). In addition, this cocktail treatment was more effective at reducing Aβ42 levels than Aβ40 levels in the mNotch$^{\Delta E}$-N2a cells.

DISCUSSION

Cocktail treatment consists of multiple drugs targeting different sites of action or molecules. It is expected to have an additive or synergistic benefit for therapy and reduce the amount of side effects. This method has been used in an effective manner for AIDS therapy to stop or slow the growth and multiplication of the human immunodeficiency virus and has successfully lowered mortality rates so far. In this study, we have shown that a new pharmacological approach reduces Aβ levels efficiently without adverse effects. This approach is based on the combination of four drugs, β- and γ-secretase inhibitors, NSAID, and statin, targeting distinct processes of Aβ production. The four-drug cocktail reduced Aβ42 levels in the conditioned media of APP$_{NL}$-H4 and mNotch$^{\Delta E}$-N2a cells. A relative increase in Aβ42 levels causes the accumulation and oligomerization of Aβ42 in the limbic and association cortices in dominantly inherited and sporadic AD; the formation of Aβ42 oligomers is implicated in synaptic dysfunction (Selkoe, 2002). Immunization of APP transgenic mice with synthetic human-type Aβ42 resulted in the removal of Aβ deposits from the brain (Schenk et al., 1999) and could lead to a reversal of cognitive deficits (Morgan et al., 2000). Thus, inhibition of the production and deposition of Aβ42 represents a straightforward strategy for the prevention and therapy of AD.

Both β- and γ-secretase inhibitors are capable of efficiently reducing Aβ levels, even if they are used

solely; therefore, the development of secretase inhibitors is an attractive target for therapeutic intervention in AD (Mattson, 2004; Marks and Berg, 2008; Figs. 2–4). However, these secretase inhibitors preferentially inhibit the production of Aβ40 rather than that of Aβ42, resulting in a significant increase in the Aβ42/Aβ40 ratio (Fig. 4). These results are not attributed to the intrinsic nature of the secretase inhibitors used in the present study. In fact, similar results were obtained with other secretase inhibitors (e.g., the β-secretase inhibitor KMI-429 and the γ-secretase inhibitors DAPT and L-685,458; data not shown). In addition, the increase in Aβ levels by a low-dose treatment with the γ-secretase inhibitor, the "Aβ rise" (Shen and Kelleher, 2007; Burton et al., 2008), was observed in mNotch$^{\Delta E}$-N2a cells (Fig. 5). However, the mechanistic details on why secretase inhibitors show a difference in inhibitory activity between Aβ42 and Aβ40 and why γ-secretase inhibitors cause the Aβ rise remain unclear. Given the genetic knowledge on the *PS* gene (Shen and Kelleher, 2007; Wolfe, 2007) and recent studies indicating that Aβ40 inhibits Aβ42 aggregation in vitro and amyloid deposition in vivo (Kim et al., 2007), the administration of β- or γ-secretase inhibitors alone should be conducted cautiously.

NSAIDs are used primarily to treat inflammation, mild-to-moderate pain, and fever by blocking the activity of cyclooxygenase (COX). Interestingly, some NSAIDs directly alter γ-secretase activity to selectively lower Aβ42 levels accompanied by an increase in Aβ38 levels (Weggen et al., 2001; Eriksen et al., 2003). Beyond that, these NSAIDs have no effect on Notch processing (Weggen et al., 2001); consequently, they represent a promising therapeutic agent for AD (Kukar and Golde, 2008). Sulindac sulfide was efficacious in the decrease of Aβ42 levels as well as an increase in the levels of Aβ38 (Figs. 1, 4b,d). This effect of sulindac sulfide was more powerful than observed for indomethacin in APP$_{NL}$-H4 cells (100 μM: sulindac sulfide decreased Aβ42 levels by 84.2% and the ratio of Aβ42/Aβ40 by 72.0%, whereas indomethacin decreased Aβ42 levels by 36.7% and the ratio of Aβ42/Aβ40 by 12.9%; data not shown). As also observed in previous studies (Weggen et al., 2001; Eriksen et al., 2003), the administration of sulindac sulfide alone lowered the Aβ42/Aβ40 ratio in APP$_{NL}$-H4 cells (78.7% ± 3.2% vs. vehicle-treated group; Fig. 4c). The underlying mechanism for the modulation of γ-secretase activity by NSAIDs is emerging: One paper proposed that NSAIDs have an allosteric effect on PS1, which is the protease-active center molecule of γ-secretase, and alter the interaction of PS1-APP by changing the conformation of PS1 (Lleó et al., 2004). NSAIDs also directly bind to the Aβ region of APP to alter the production of Aβ42 and inhibit the aggregation of Aβ (Kukar et al., 2008). Whether NSAIDs target the enzyme, substrate, or both, sulindac sulfide, which is an Aβ42-lowering NSAID, did not compete with the γ-secretase inhibitor (Fig. 3b). At 10^{-9} to 10^{-7} M of the γ-secretase inhibitor, their coadministration significantly reduced the levels of Aβ42 compared with the administration of the γ-secretase inhibitor alone. These results suggest that coadministration is more effective than administration alone.

Statins are drugs that are widely used to lower cholesterol levels. They inhibit the activity of HMG-CoA reductase, which is the rate-limiting enzyme of the mevalonate pathway of cholesterol synthesis. Because Aβ generation occurs in specialized cholesterol-rich membrane subdomains, the cellular cholesterol level appears to be closely associated with Aβ generation (Kaether and Haass, 2004). Namely, a low level of intracellular cholesterol stimulates the nonamyloidogenic pathway, in which α-secretase is involved (Simons et al., 2001). The reason why simvastatin showed little effect on Aβ40 levels in the presence of the γ-secretase inhibitor in the present study remains unclear (Fig. 3a), whereas coadministration with either the β- or the γ-secretase inhibitor efficiently reduced Aβ42 levels (Figs. 2b, 3b). Moreover, statins have provided a new therapeutic concept for the treatment of neuroinflammatory diseases because of their potency in altering GTPase-mediated signaling relevant to inflammatory processes (Zipp et al., 2007). Because amyloid plaques in AD are accompanied by a localized inflammatory response, statins might also be useful drugs because they interfere with the induction of tumor necrosis factor-α and inducible nitric oxide synthase in astrocytic and microglial cell cultures (Blennow et al., 2006; Zipp et al., 2007; Marks and Berg, 2008).

The efficacy of cocktail treatment should be determined by the additive or synergistic effect of drugs and its ability to alleviate possible adverse side effects that may be caused by individual drugs. Our four-drug cocktail significantly reduced Aβ levels, with no change in Notch processing in APP$_{NL}$-H4 and mNotch$^{\Delta E}$-N2a cells (Figs. 4, 5). The theoretical values estimated by the multiplication of the data of each single drug treatment for the inhibitory efficacies of Aβ production are 23.0% (Aβ40) and 35.4% (Aβ42; Fig. 4a,b). These results were close to the values of four-drug cocktail treatment (Aβ40, 23.8%; Aβ42, 28.3%; Fig. 4a,b). It is suggested that the four drugs used in the present study did not interfere with each other in the suppression of Aβ production. Another important point is that the four-drug cocktail treatment did not affect Notch processing accompanied by significant reduction in Aβ levels (Fig. 5). In contrast, the administration of γ-secretase inhibitor alone exerted its effects on the processing of both APP and Notch (Fig. 5). It follows from these results that this four-drug cocktail did not inhibit the processing of Notch and would have few side effects.

In the present study, we focused on drugs that influence Aβ production. Several drugs have been developed to reduce Aβ levels according to the amyloid hypothesis (Walker et al., 2005; Blennow et al., 2006; Marks and Berg, 2008). For example, α-secretase activators are potential drugs that have two dimensions to their action, because α-secretase cleaves within the Aβ region of APP, leading to a reduction in Aβ levels and

the generation of sAPPα that has neuroprotective effects. For the Aβ-degradation system, Saito et al. (2005) reported that the neuropeptide somatostatin regulates Aβ catabolism by modulating the activity and localization of neprilysin, which is a major enzyme responsible for the degradation of Aβ (Iwata et al., 2001). Therefore, somatostatin receptors might be new pharmacological target molecules for the prevention and treatment of AD (Iwata et al., 2005; Saido and Iwata, 2006). For the Aβ-clearance system (Aβ efflux system from the brain parenchyma to peripheral blood), it is becoming clear that a particularly promising approach for the removal of Aβ is to use the power and specificity of the immune system to eliminate excess Aβ in the brain (Town, 2009). Although immunization with Aβ resulted in clearance of amyloid plaques in the brains of AD patients, the clearance did not present significant improvement of the patients' cognitive functions. It is thought that one of major causes that have driven Aβ immunotherapy into failure may be targeting to eliminate amyloid plaques per se. Increasing evidence has indicated that particular forms of soluble Aβ, such as oligomeric froms, but not insoluble Aβ, may be one of major causes leading to neuronal dysfunction and further cognitive impairment (Haass and Selkoe, 2007). Thus, it is suggested that it may be necessary to inhibit newly produced Aβ, which forms soluble oligomers. In addition, compounds capable of disaggregating Aβ or inhibiting Aβ aggregation (formation of low-molecular-weight oligomers and fibrils) are pharmacological strategies that could be used in the treatment of AD. Recently, it was reported that the reduction of pyroglutamate-modified Aβ by inhibition of glutaminyl cyclase offered an attenuation of AD-like pathology in AD model mice and a new *Drosophila* model (Schilling et al., 2008). Large numbers of drugs have been developed in recent years, and numerous options for combinatorial therapies are available to reduce Aβ levels without leading to adverse effects, such as the impairment of Notch processing, as shown here. Some clinical trials of an Aβ-targeting compound have failed (for example, *R*-flurbiprofen; Green et al., 2009). However, almost all of the compounds have been administered alone. Our data suggest that administration of a combination of drugs consisting of Aβ-lowering drugs at low doses such as our four-drug cocktail might be an effective approach by which to prevent, delay, slow, and treat AD. This cocktail strategy may be extended to targeting the other downstream pathological processes of AD, such as tauopathy, oxidative stress, inflammation, neuronal loss, and neuronal cell death, to achieve maximal effects (Saido and Iwata, 2006). We suggest that a transition might be coming from the time when a single drug is developed and evaluated to the time when multiple drugs are designed.

ACKNOWLEDGMENTS

We thank Dr. Raphael Kopan (Washington University) for providing the plasmid of mNotch$^{\Delta E}$ and Mr. Sosuke Yagishita (The University of Tokyo) for his valuable technical advice.

REFERENCES

Asai M, Hattori C, Iwata N, Saido TC, Sasagawa N, Szabó B, Hashimoto Y, Maruyama K, Tanuma S, Kiso Y, Ishiura S. 2006. The novel β-secretase inhibitor KMI-429 reduces amyloid β peptide production in amyloid precursor protein transgenic and wild-type mice. J Neurochem 96:533–540.

Asai M, Iwata N, Yoshikawa A, Aizaki Y, Ishiura S, Saido TC, Maruyama K. 2007. Berberine alters the processing of Alzheimer's amyloid precursor protein to decrease Aβ secretion. Biochem Biophys Res Commun 352:498–502.

Beel AJ, Sanders CR. 2008. Substrate specificity of γ-secretase and other intramembrane proteases. Cell Mol Life Sci 65:1311–1334.

Beher D, Wrigley JD, Nadin A, Evin G, Masters CL, Harrison T, Castro JL, Shearman MS. 2001. Pharmacological knock-down of the presenilin 1 heterodimer by a novel γ-secretase inhibitor: implications for presenilin biology. J Biol Chem 276:45394–45402.

Blennow K, de Leon MJ, Zetterberg H. 2006. Alzheimer's disease. Lancet 368:387–403.

Burton CR, Meredith JE, Barten DM, Goldstein ME, Krause CM, Kieras CJ, Sisk L, Iben LG, Polson C, Thompson MW, Lin XA, Corsa J, Fiedler T, Pierdomenico M, Cao Y, Roach AH, Cantone JL, Ford MJ, Drexler DM, Olson RE, Yang MG, Bergstrom CP, McElhone KE, Bronson JJ, Macor JE, Blat Y, Grafstrom RH, Stern AM, Seiffert DA, Zaczek R, Albright CF, Toyn JH. 2008. The amyloid-β rise and γ-secretase inhibitor potency depend on the level of substrate expression. J Biol Chem 283:22992–23003.

De Strooper B, Annaert W, Cupers P, Saftig P, Craessaerts K, Mumm JS, Schroeter EH, Schrijvers V, Wolfe MS, Ray WJ, Goate A, Kopan R. 1999. A presenilin-1-dependent γ-secretase-like protease mediates release of Notch intracellular domain. Nature 398:518–522.

Dominguez D, Tournoy J, Hartmann D, Huth T, Cryns K, Deforce S, Serneels L, Camacho IE, Marjaux E, Craessaerts K, Roebroek AJ, Schwake M, D'Hooge R, Bach P, Kalinke U, Moechars D, Alzheimer C, Reiss K, Saftig P, De Strooper B. 2005. Phenotypic and biochemical analyses of BACE1- and BACE2-deficient mice. J Biol Chem 280:30797–30806.

Eriksen JL, Sagi SA, Smith TE, Weggen S, Das P, McLendon DC, Ozols VV, Jessing KW, Zavitz KH, Koo EH, Golde TE. 2003. NSAIDs and enantiomers of flurbiprofen target γ-secretase and lower Aβ42 in vivo. J Clin Invest 112:440–449.

Fassbender K, Simons M, Bergmann C, Stroick M, Lutjohann D, Keller P, Runz H, Kuhl S, Bertsch T, von Bergmann K, Hennerici M, Beyreuther K, Hartmann T. 2001. Simvastatin strongly reduces levels of Alzheimer's disease β-amyloid peptides Aβ42 and Aβ40 in vitro and in vivo. Proc Natl Acad Sci U S A 98:5856–5861.

Geling A, Steiner H, Willem M, Bally-Cuif L, Haass C. 2002. A γ-secretase inhibitor blocks Notch signaling in vivo and causes a severe neurogenic phenotype in zebrafish. EMBO Rep 3:688–694.

Green RC, Schneider LS, Amato DA, Beelen AP, Wilcock G, Swabb EA, Zavitz KH,Tarenflurbil Phase 3 Study Group. 2009. Effect of tarenflurbil on cognitive decline and activities of daily living in patients with mild Alzheimer disease: a randomized controlled trial. JAMA 302:2557–25564.

Haass C, Selkoe DJ. 2007. Soluble protein oligomers in neurodegeneration: lessons from the Alzheimer's amyloid β-peptide. Nat Rev Mol Cell Biol 8:101–112.

Imamura Y, Watanabe N, Umezawa N, Iwatsubo T, Kato N, Tomita T, Higuchi T. 2009. Inhibition of γ-secretase activity by helical β-peptide foldamers. J Am Chem Soc 131:7353–7359.

Iwata N, Tsubuki S, Takaki Y, Shirotani K, Lu B, Gerard NP, Gerard C, Hama E, Lee HJ, Saido TC. 2001. Metabolic regulation of brain Aβ by neprilysin. Science 292:1550–1552.

Iwata N, Higuchi M, Saido TC. 2005. Metabolism of amyloid-β peptide and Alzheimer's disease. Pharmacol Ther 108:129–148.

Kaether C, Haass C. 2004. A lipid boundary separates APP and secretases and limits amyloid β-peptide generation. J Cell Biol 167:809–812.

Kim J, Onstead L, Randle S, Price R, Smithson L, Zwizinski C, Dickson DW, Golde T, McGowan E. 2007. Aβ40 inhibits amyloid deposition in vivo. J Neurosci 27:627–633.

Kopan R, Schroeter EH, Weintraub H, Nye JS. 1996. Signal transduction by activated mNotch: importance of proteolytic processing and its regulation by the extracellular domain. Proc Natl Acad Sci U S A 93:1683–1688.

Kukar T, Golde TE. 2008. Possible mechanisms of action of NSAIDs and related compounds that modulate γ-secretase cleavage. Curr Top Med Chem 8:47–53.

Kukar TL, Ladd TB, Bann MA, Fraering PC, Narlawar R, Maharvi GM, Healy B, Chapman R, Welzel AT, Price RW, Moore B, Rangachari V, Cusack B, Eriksen J, Jansen-West K, Verbeeck C, Yager D, Eckman C, Ye W, Sagi S, Cottrell BA, Torpey J, Rosenberry TL, Fauq A, Wolfe MS, Schmidt B, Walsh DM, Koo EH, Golde TE. 2008. Substrate-targeting γ-secretase modulators. Nature 453:925–929.

Lleó A, Berezovska O, Herl L, Raju S, Deng A, Bacskai BJ, Frosch MP, Irizarry M, Hyman BT. 2004. Nonsteroidal anti-inflammatory drugs lower $A\beta_{42}$ and change presenilin 1 conformation. Nat Med 10:1065–1066.

Marks N, Berg MJ. 2008. Neurosecretases provide strategies to treat sporadic and familial Alzheimer disorders. Neurochem Int 52:184–215.

Mattson MP. 2004. Pathways towards and away from Alzheimer's disease. Nature 430:631–639.

Morgan D, Diamond DM, Gottschall PE, Ugen KE, Dickey C, Hardy J, Duff K, Jantzen P, DiCarlo G, Wilcock D, Connor K, Hatcher J, Hope C, Gordon M, Arendash GW. 2000. Aβ peptide vaccination prevents memory loss in an animal model of Alzheimer's disease. Nature 408:982–985.

Saido TC, Iwata N. 2006. Metabolism of amyloid β peptide and pathogenesis of Alzheimer's disease. Towards presymptomatic diagnosis, prevention and therapy. Neurosci Res 54:235–253.

Saito T, Iwata N, Tsubuki S, Takaki Y, Takano J, Huang SM, Suemoto T, Higuchi M, Saido TC. 2005. Somatostatin regulates brain amyloid β peptide $A\beta_{42}$ through modulation of proteolytic degradation. Nat Med 11:434–439.

Schenk D, Barbour R, Dunn W, Gordon G, Grajeda H, Guido T, Hu K, Huang J, Johnson-Wood K, Khan K, Kholodenko D, Lee M, Liao Z, Lieberburg I, Motter R, Mutter L, Soriano F, Shopp G, Vasquez N, Vandevert C, Walker S, Wogulis M, Yednock T, Games D, Seubert P. 1999. Immunization with amyloid-β attenuates Alzheimer-disease-like pathology in the PDAPP mouse. Nature 400:173–177.

Schilling S, Zeitschel U, Hoffmann T, Heiser U, Francke M, Kehlen A, Holzer M, Hutter-Paier B, Prokesch M, Windisch M, Jagla W, Schlenzig D, Lindner C, Rudolph T, Reuter G, Cynis H, Montag D, Demuth HU, Rossner S. 2008. Glutaminyl cyclase inhibition attenuates pyroglutamate Aβ and Alzheimer's disease-like pathology. Nat Med 14:1106–1111.

Seiffert D, Bradley JD, Rominger CM, Rominger DH, Yang F, Meredith JE Jr, Wang Q, Roach AH, Thompson LA, Spitz SM, Higaki JN, Prakash SR, Combs AP, Copeland RA, Arneric SP, Hartig PR, Robertson DW, Cordell B, Stern AM, Olson RE, Zaczek R. 2000. Presenilin-1 and -2 are molecular targets for γ-secretase inhibitors. J Biol Chem 275:34086–34091.

Selkoe DJ. 2002. Alzheimer's disease is a synaptic failure. Science 298:789–791.

Shearman MS, Beher D, Clarke EE, Lewis HD, Harrison T, Hunt P, Nadin A, Smith AL, Stevenson G, Castro JL. 2000. L-685,458, an aspartyl protease transition state mimic, is a potent inhibitor of amyloid β-protein precursor γ-secretase activity. Biochemistry 39:8698–8704.

Shen J, Kelleher RJ 3rd. 2007. The presenilin hypothesis of Alzheimer's disease: evidence for a loss-of-function pathogenic mechanism. Proc Natl Acad Sci U S A 104:403–409.

Simons M, Keller P, Dichgans J, Schulz JB. 2001. Cholesterol and Alzheimer's disease: is there a link? Neurology 57:1089–1093.

Stachel SJ, Coburn CA, Steele TG, Jones KG, Loutzenhiser EF, Gregro AR, Rajapakse HA, Lai MT, Crouthamel MC, Xu M, Tugusheva K, Lineberger JE, Pietrak BL, Espeseth AS, Shi XP, Chen-Dodson E, Holloway MK, Munshi S, Simon AJ, Kuo L, Vacca JP. 2004. Structure-based design of potent and selective cell-permeable inhibitors of human β-secretase (BACE-1). J Med Chem 47:6447–6450.

Town T. 2009. Alternative Aβ immunotherapy approaches for Alzheimer's disease. CNS Neurol Disord Drug Targets 8:114–127.

Walker LC, Ibegbu CC, Todd CW, Robinson HL, Jucker M, LeVine H 3rd, Gandy S. 2005. Emerging prospects for the disease-modifying treatment of Alzheimer's disease. Biochem Pharmacol 69:1001–1008.

Weggen S, Eriksen JL, Das P, Sagi SA, Wang R, Pietrzik CU, Findlay KA, Smith TE, Murphy MP, Bulter T, Kang DE, Marquez-Sterling N, Golde TE, Koo EH. 2001. A subset of NSAIDs lower amyloidogenic Aβ42 independently of cyclooxygenase activity. Nature 414:212–216.

Weggen S, Rogers M, Eriksen J. 2007. NSAIDs: small molecules for prevention of Alzheimer's disease or precursors for future drug development. Trends Pharmacol Sci 28:536–543.

Willem M, Garratt AN, Novak B, Citron M, Kaufmann S, Rittger A, De Strooper B, Saftig P, Birchmeier C, Haass C. 2006. Control of peripheral nerve myelination by the β-secretase BACE1. Science 314:664–666.

Wolfe MS. 2007. When loss is gain: reduced presenilin proteolytic function leads to increased Aβ42/Aβ40. Talking point on the role of presenilin mutations in Alzheimer disease. EMBO Rep 8:136–140.

Wong GT, Manfra D, Poulet FM, Zhang Q, Josien H, Bara T, Engstrom L, Pinzon-Ortiz M, Fine JS, Lee HJ, Zhang L, Higgins GA, Parker EM. 2004. Chronic treatment with the γ-secretase inhibitor LY-411,575 inhibits β-amyloid peptide production and alters lymphopoiesis and intestinal cell differentiation. J Biol Chem 279:12876–12882.

Zipp F, Waiczies S, Aktas O, Neuhaus O, Hemmer B, Schraven B, Nitsch R, Hartung HP. 2007. Impact of HMG-CoA reductase inhibition on brain pathology. Trends Pharmacol Sci 28:342–349.

Neurobiology of Disease

A Noncompetitive BACE1 Inhibitor TAK-070 Ameliorates Aβ Pathology and Behavioral Deficits in a Mouse Model of Alzheimer's Disease

Hiroaki Fukumoto,[1]* Hideki Takahashi,[1]* Naoki Tarui,[1] Junji Matsui,[1] Taisuke Tomita,[2] Mitsuhiro Hirode,[1] Masumi Sagayama,[1] Ryouta Maeda,[1] Makiko Kawamoto,[1] Kazuko Hirai,[1] Jun Terauchi,[1] Yasufumi Sakura,[1] Mitsuru Kakihana,[1] Kaneyoshi Kato,[1] Takeshi Iwatsubo,[2,3] and Masaomi Miyamoto[1]

[1]Pharmaceutical Research Division, Takeda Pharmaceutical Company Limited, Yodogawa-ku, Osaka 532-8686, Japan, and [2]Department of Neuropathology and Neuroscience, Graduate School of Pharmaceutical Sciences, and [3]Department of Neuropathology, Graduate School of Medicine, The University of Tokyo, Bunkyo-ku, Tokyo 113-0033, Japan

We discovered a nonpeptidic compound, TAK-070, that inhibited BACE1, a rate-limiting protease for the generation of Aβ peptides that are considered causative for Alzheimer's disease (AD), in a noncompetitive manner. TAK-070 bound to full-length BACE1, but not to truncated BACE1 lacking the transmembrane domain. Short-term oral administration of TAK-070 decreased the brain levels of soluble Aβ, increased that of neurotrophic sAPPα by ~20%, and normalized the behavioral impairments in cognitive tests in Tg2576 mice, an APP transgenic mouse model of AD. Six-month chronic treatment decreased cerebral Aβ deposition by ~60%, preserving the pharmacological efficacy on soluble Aβ and sAPPα levels. These results support the feasibility of BACE1 inhibition with a noncompetitive inhibitor as disease-modifying as well as symptomatic therapy for AD.

Introduction

The accumulation of amyloid-β peptides (Aβ) in the brain is strongly implicated in the pathogenesis of Alzheimer's disease (AD), and considered as a prime target for the disease-modifying therapy of AD (Selkoe and Schenk, 2003). Aβ is proteolytically produced through sequential cleavages by β- and γ-secretases from amyloid precursor protein (APP). The β-secretase cleavage of APP is executed by a membrane-bound aspartic protease, β-site APP-cleaving enzyme 1 (BACE1), which is considered to be the rate-limiting step in the production of Aβ (Cole and Vassar, 2008), whereas a majority of APP is cleaved by α-secretase at the midportion of Aβ sequence in a way to preclude Aβ production, by competing with BACE1.

γ-Secretase generates the C termini of Aβ with different length, e.g., $Aβ_{40}$ or $Aβ_{42}$, the latter being considered as the pathogenic species (Iwatsubo et al., 1994). Inhibition of γ-secretase may potentially cause side effects, because genetic knock-out (KO) of presenilin 1 and 2, the catalytic subunits of γ-secretase, leads to embryonic lethality due to failure in activation of Notch, which is essential for development and differentiation (Shen et al., 1997; Wong et al., 1997; Donoviel et al., 1999). Furthermore, cognitive deficits associated with synaptic degeneration have been documented in PS1/PS2 conditional KO mice with or without APP transgenic background (Saura et al., 2004, 2005; Chen et al., 2008). In contrast, BACE1 KO mice do not show such fatal phenotypes despite its complete ablation, except for partial hypomyelination at the developmental stage (Hu et al., 2006; Sankaranarayanan et al., 2008) or schizophrenia-like behavior in homozygous BACE1 KO mice (Savonenko et al., 2008), whereas cognitive deficits are ameliorated on APP transgenic background (Ohno et al., 2004, 2006, 2007). Furthermore, it has been well documented that the protein levels or activities of BACE1 are upregulated in the brains of patients with sporadic AD (Stockley and O'Neill, 2007). Therefore, BACE1 is considered as a promising target for the mechanism-based therapy for AD. So far, several BACE1 inhibitors have been reported (Hussain et al., 2007; Sankaranarayanan et al., 2009; Silvestri, 2009), although no compound that is orally active and highly penetrable to brain tissues with functional ameliorations has been documented.

We conducted a cell-based assay in the IMR32 human neuroblastoma cell line for small chemical compounds that reduce the secretion of Aβ and increase that of sAPPα, the latter being recognized as neurotrophic with ameliorative effects on cognitive behaviors (Isacson et al., 2002; Postina, 2008). Finally we discovered a nonpeptidic compound, (*R*)-6-[(1,1′-biphenyl)-4-ylmethoxy]-1,2,3,4-tetrahydro-*N*,*N*-dimethyl-2-naphthalene-ethan-amine hydrochloride monohydrate (TAK-070) (Fig. 1), as a novel noncompetitive BACE1 inhibitor. TAK-070 ameliorated Aβ pathology and behavioral deficits in Tg2576, an APP transgenic model mice of AD, although the reduction in Aβ levels was modest,

Received June 7, 2010; accepted June 30, 2010.

We thank the Mayo Clinic for supplying the Tg2576 mice, Kozo Shimakawa for breeding the Tg2576 mice, Satoko Osawa for technical assistance, Dr. Gopal Thinakaran for valuable advice, and Drs. Zen-ichi Terashita, Yasuhiro Sumino, and Shigenori Ohkawa for continuous support to the study.

*H.F. and H.T. contributed equally to this work.

All authors except for T. Tomita and T. Iwatsubo are employees of Takeda Pharmaceutical Company, which was engaged in the research of BACE1 inhibitors for potential use as AD therapeutics.

Correspondence should be addressed to Dr. Hiroaki Fukumoto, Pharmaceutical Research Division, Takeda Pharmaceutical Company Limited, 2-17-85 Juso-honmachi, Yodogawa-ku, Osaka 532-8686, Japan. E-mail: Fukumoto_Hiroaki@takeda.co.jp.

DOI:10.1523/JNEUROSCI.2884-10.2010

 0270-6474/10/3011157-10$15.00/0

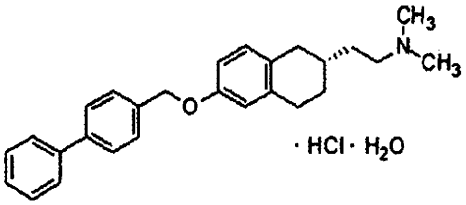

Figure 1. Chemical structure of TAK-070.

unlike those observed by complete ablation of BACE1. We propose that the partial reduction in Aβ as well as increase in sAPPα by a noncompetitive BACE1 inhibition may be sufficient to modify amyloid pathology and ameliorate cognitive deficits, without causing potential adverse events by complete BACE1 ablation.

Materials and Methods

Compound

The chemical TAK-070 was made by Takeda Pharmaceutical Company Limited (Takeda), and the chemical structure is shown in Figure 1. The chemical synthesis and related information are described in the patent of JP-A 11-80098 (*WO98/38156*). γ-Secretase inhibitor IX (DAPT) was purchased from Calbiochem.

Cell cultures and sample preparation

IMR32 human neuroblastoma cell line was obtained from American Type Culture Collection (ATCC), and mouse Neuro-2a neuroblastoma cells stably expressing human Swedish mutant APP (N2aAPPsw cells) were generated as described previously (Tomita et al., 2002). For ELISA analysis, cells were cultured on 48-well multi-plates at 5×10^4 cells/cm^2 to reach near total confluence in DMEM (Nikken Biomedical Laboratory) supplemented with 10% (v/v) heat-inactivated fetal bovine serum (FBS) (Wako) in a humid atmosphere containing 10% CO_2. The culture medium was replaced with DMEM/0.2% bovine serum albumin (BSA) (Wako) containing various concentrations of TAK-070, and the cells were cultured for 24 h. The conditioned media were subjected to ELISA quantitation.

Quantitation of sAPPα and Aβ by ELISA

To quantitate human sAPPα, we used LN27 that recognizes the N-terminal portion of APP (Zymed) as a capture antibody. ELISA plates (high binding, clear plate, Greiner) were filled with LN27 (0.5 μg/ml, 75 μl/well) in carbonated buffer (100 mmol/L, pH 9.6) and incubated at 4°C overnight. After washing the plates with PBS (Invitrogen) three times, each well was blocked with 100 μl of BlockAce solution (Dai-Nippon) diluted fourfold (v/v) for >2 h. After washing the plates with PBS twice, 50 μl samples or standards prepared from conditioned media containing sAPPα were mixed with 50 μl of buffer A (20 mmol/L phosphate buffer, pH 7.2, 10% BlockAce, 0.2% protease-free BSA, 0.05% thimerosal, 0.4 mol/L NaCl, 0.076% CHAPS, 2 mmol/L EDTA-2Na, 0.2% SDS, and 4 mmol/L DTT) in each well. Buffer A contains DTT to break the S-S bond of sAPPα to enhance the recognition by the LN27 antibody. The mixture was incubated in the plate overnight at 4°C. After washing the plates with PBS four times, BAN50-HRP (75 μl/well) [which recognizes the C-terminal portion of human sAPPα (Asami-Odaka et al., 1995)] diluted in the detection buffer (20 mmol/L phosphate buffer, pH 7.2, 1% protease-free BSA, 2 mmol/L EDTA-2Na, 0.05% thimerosal, and 0.4 mol/L NaCl) was added to each well. The plates were incubated at room temperature for 3–4 h. After washing the plates with PBS six times, substrates were added and the reaction mixtures were developed. To measure sAPPα in brain lysates, the homogenate buffer free of detergents was used to preclude contamination of membrane-associated APP.

$A\beta_{40}$ or $A\beta_{42}$ was quantitated by two-site sandwich ELISA using a capture antibody BNT77, which recognizes the midportion of Aβ without detecting $A\beta_{17\text{-}40/42}$ (i.e., the cleaved products by α- and γ-secretases) (Fukumoto et al., 1999), and the detector antibodies of BA27-HRP or BC05-HRP that specifically detect the C termini of $A\beta_{40}$ or $A\beta_{42}$, respectively, as described previously (Asami-Odaka et al., 1995). TMB substrate (Pierce) was used as a chromogenic substrate. After stopping the reaction with phosphoric acid solution (1 mol/L, 75 μl/well), the enzymatic products were measured using a multi-label counter at OD450 (WALLAC Arvo Sx; PerkinElmer Life Sciences).

Immunoblot analysis

Quantification of the levels of sAPPβ, sAPPα, APP, APP C-terminal fragment (CTF) (e.g., C83 and C99), BACE, or ADAM10 was performed on conditioned media or cell lysates of N2aAPPsw cells treated with vehicle DMSO (0.1% v/v), 3 μmol/L TAK-070, or 3 μmol/L DAPT for 24 h. SeeBlue Plus2 (Invitrogen) was used as a molecular weight standard. Protein samples separated by SDS-PAGE were electrophoretically transferred to an Immobilon PVDF membrane (Millipore). The membranes were blocked with 5% (w/v) skim milk solution (Wako) in TBS-T (20 mmol/L Tris-buffer, pH 7.0, containing 50 mmol/L NaCl and 0.1% Tween 20) and reacted overnight with a detector antibody. The following monoclonal or polyclonal antibodies were used: monoclonal antibodies that specifically react with the C terminus of Swedish mutant sAPPβ (sAPPβsw) [clone 6A1, IBL, 1:100 dilution (Lakshmana et al., 2009)], the C terminus of human sAPPα [BAN50, Takeda, 0.5 μg/ml (Asami-Odaka et al., 1995)], α-tubulin (clone AA4.3, Developmental Studies Hybridoma Bank, cultured medium from hybridoma), respectively, and polyclonal antibodies to the C terminus of APP [APP(C), No. 18961; IBL, 1:1000 dilution] that detect total APP and APP-CTFs, anti-mouse/rat APP [APP(597), No. 28055; IBL, 1:1000 dilution] raised against the C-terminal 16 aa of rodent sAPPα that specifically recognizes rodent, but not human, sAPPα, anti-sAPPβ [No. 18957; IBL, 1:100 dilution (Lakshmana et al., 2009)] specific for sAPPβ derived from wild-type APP (sAPPβwt), ADAM10 (735–749) (No. 422751; Calbiochem, 0.5 μg/ml), and the C terminus of BACE1 (No. 28051; IBL, 0.1 μg/ml, 1:200). Specificity of anti-human/mouse APP antibodies is shown in supplemental Figure S1 (available at www.jneurosci.org as supplemental material). The hybridoma clone AA4.3 was obtained from the Developmental Studies Hybridoma Bank developed under the auspices of the National Institute of Child Health and Human Development and maintained by The University of Iowa, Department of Biology (Iowa City, IA). After washing with TBS-T, the membranes were further incubated with TBS (20 mmol/L Tris-buffer, pH 7.0, containing 50 mmol/L NaCl) buffer containing an anti-mouse IgG antibody-HRP (1/5000) for a monoclonal antibody or an anti-rabbit IgG antibody-HRP (1/5000) (GE Healthcare) for polyclonal antibodies. The membranes were washed with TBS-T, and then immunoreactive bands were visualized using Immunostar, Immunostar LD (Wako), or SuperSignal West Femto Maximum Sensitivity Substrate (Thermo Scientific) according to the manufacturer's instructions. The intensity of bands on the membrane was captured and quantitated using LAS-1000plus (FUJIFILM).

Cell-based assay for α-secretase activity

The assay (Doedens et al., 2003) was performed with a slight modification. N2aAPPsw cells were cultured in DMEM supplemented with 10% FCS until grown to confluence. The cells were collected by PBS (−) (Ca^{2+}, Mg^{2+} free) buffer and centrifuged for 5 min at 300 × *g*. After washing with PBS (−), the cells were suspended in PBS (−) at a final concentration of 4×10^7 cells/ml. The enzymatic reaction was initiated by combining an equal volume (100 μl) of cell suspension and reaction mixture at a final cell concentration of 2×10^7 cells/ml, 10 μmol/L each of leupeptin (Peptide Institute), aprotinin (Roche Diagnostics), and α-secretase fluorogenic substrate [MCA-HQKLVFFA (K-DNP), BioSource], with vehicle of DMSO, TAK-070 (final concentration: 3 μmol/L), or (−)-epigallocatechin-3-gallate (catechin, Wako) (final concentration: 20 μmol/L). After each incubation time point, the cells were centrifuged, the cell-free supernatants of each 100 μl were added to a 96-well black plate (Greiner), and fluorescence intensity after cleavage by α-secretase was measured (excitation 320 nm, emission 400 nm) (WALLAC Arvo Sx; PerkinElmer Life Sciences).

Expression and purification of FLAG-tagged full-length BACE1 or truncated BACE1 (1-454)

The plasmid containing cDNA encoding the entire coding frame of human BACE1 (clone No. FG04087) was obtained from KAZUSA DNA Research

Institute. The full-length BACE1 (1-501) and C-terminally truncated BACE1 (1-454, 460, 465, 471 and 474) lacking the transmembrane domain were cloned into pcDNA3.1 (−) (Invitrogen) vector with a C-terminal FLAG tag [pcDNA3.1(−)BACE1-flag and pcDNA3.1(−)BACE1(1-454, 460, 465, 471, or 474)-flag, respectively]. COS-7 cells were cultured in DMEM supplemented with 10% (v/v) heat-inactivated FBS at 37°C in a humid atmosphere of 5% CO_2. Cells were grown in an F225 cell culture flask (225 cm^2) and transfected with 22.5 μg of pcDNA3.1(−)BACE1-flag or pcDNA3.1(−)BACE1(1-454, 460, 465, 471, or 474)-flag, using Fugene6 (Roche Diagnostics). Forty-eight hours after transfection, cells were scraped in PBS and centrifuged for 10 min at 1870 × *g*. The supernatant was used as a source for further purification of the truncated BACE1 (1-454, 460, or 465). To purify full-length BACE1 or truncated BACE1 (1-471 or 474), the pellet was resuspended in 50 mmol/L Tris-HCl buffer, pH 7.4, containing 0.15 mol/L NaCl, 1 mmol/L EDTA, and 0.1 mmol/L PMSF. The cells were disrupted by sonication and centrifuged at 1870 × *g* for 10 min. The supernatant was centrifuged at 100,000 × *g* for 45 min to yield crude membrane pellets. The membrane was solubilized in 50 mmol/L Tris-HCl buffer, pH 7.4, containing 50 mmol/L octyl-β-glucoside, 0.15 mol/L NaCl, 1 mmol/L EDTA, and 0.1 mmol/L PMSF at 4°C for 2 h, centrifuged at 100,000 × *g* for 45 min. The fractions containing full-length of BACE1, C-terminally truncated BACE1 (1-454, 460, 465, 471, or 474) fused with FLAG tag were then loaded on an Anti-FLAG M2 affinity gel (Sigma) column. The column was washed with 50 mmol/L Tris-HCl buffer, pH 7.4, containing 0.15 mol/L NaCl, and purified FLAG-tagged recombinant BACE1 proteins were obtained by elution with 100 μg/ml FLAG peptides.

Cell-free assay for BACE1 activity

A statine substrate analog inhibitor PI (TEEISEVNXVAEF; X = statine) (Sinha et al., 1999) and the fluorogenic substrate for BACE1 [Nma-SEVKMDAEK(Dnp)RR-NH_2] were purchased from the Peptide Institute. The substrate was dissolved in 125 mmol/L acetic acid. TAK-070 and PI were dissolved in dimethylformamide (DMF). Assays were performed in black 96-well microplates (Greiner) in a final volume of 50 μl. Each well contained 25 μl of acetate buffer (pH 5.5, 50 mmol/L), 10 μl of recombinant BACE1, 10 μl of substrate (250 μmol/L), and 5 μl of various concentrations of compounds at a final DMF concentration of 0.5%. The assay mixtures were incubated at 37°C for 20 h. After incubation, the fluorescence of the enzymatic product was measured at 460 nm (excitation at 325 nm) using Fluoroskan Ascent (Labsystems). The percentage of inhibition was calculated by an equation of 100 × [1 − (test − blank)/(control − blank)], where test, control, and blank are fluorescence intensities in the presence of a compound, absence of a compound, and absence of both the BACE1 enzyme and a compound, respectively. IC_{35} values were calculated by linear regression analysis using a BSAS program. To clarify the inhibition profile, double-reciprocal (Lineweaver–Burk) plot analysis was performed using 10 μl substrate of 100, 150, 250, 500, or 1000 μmol/L (a final concentration of 20, 30, 50, 100, or 200 μmol/L, respectively) and 5 μl of TAK-070 of 100 or 300 μmol/L (a final concentration of 10 or 30 μmol/L) in total assay solution of 50 μl. The reciprocal of change in the fluorescence value in the presence of TAK-070 at each concentration was plotted on the vertical axis, and the reciprocal of the substrate concentration was plotted on the longitudinal axis.

Surface plasmon resonance binding assay

We used a Biacore3000/BiacoreA100 instrument to generate sensorgrams for binding of TAK-070 onto full-length BACE1, C-terminally truncated BACE1 (1-454), (1-460), (1-465), (1-471), (1-474), APP688 [Leu18-Leu688 with a C-terminal 6-His tag, also referred to as protease nexin II containing Kunitz-type Protease Inhibitor (KPI) domain, #3466-PI, R&D Systems], and sAPPβ containing KPI domain (BACE1-cleaved N-terminal product of APP, #SIG-39938, Sigma). Each protein was immobilized on a Sensor Chip CM5 (carboxymethylated dextran matrix chip) using amine-coupling kit (Biacore). The sensorgrams were recorded at a flow rate of 30 μl/60 s in a solution of PBS containing 10% DMSO and 0.005% Surfactant P20 (Biacore) at room temperature. TAK-070 was initially dissolved in DMSO and diluted in PBS containing 0.005% Surfactant P20 at a final concentration of 0.5–8, 5, or 10 μmol/L. Specific binding to each protein was calculated as signal to each protein subtracted by signal to vehicle (DMSO).

Animals

All animals were housed in rooms maintained at 24°C with a 12 h light/dark cycle. Food (chow containing TAK-070; Oriental Yeast) and tap water were provided *ad libitum*. In each experiment, mice were randomly grouped, avoiding differences in body weight among groups. All experiments using animals were reviewed and approved by the Internal Animal Care and Use Committee of Takeda Pharmaceutical Research Laboratories.

Short-term treatment of Tg2576 by TAK-070

Female Tg2576 mice at 2 months of age were used for short-term treatment with TAK-070. Tg2576 were fed either chow containing TAK-070 (5.6 ppm or 56 ppm, corresponding to ~0.87 or 8.2 mg/kg, p.o., respectively; $n = 15$) or chow without TAK-070 ($n = 15$) for 7 weeks. Then, each mouse was decapitated and the cerebral cortex was dissected out on ice. Each sample was immediately frozen on dry ice and stored at −80°C until assay. Halves of the cerebral cortices were homogenized in ice-cold Tris-extraction buffer (50 mmol/L Tris, pH 7.2, 200 mmol/L sodium chloride, 2% protease-free bovine serum albumin, and 0.01% thimerosal) containing protease inhibitor cocktails (1 mmol/L PMSF, 40 KIU aprotinin, 10 μmol/L pepstatin A, 1 mmol/L phosphoramidon, 10 mmol/L 1,10-phenanthroline, 2 mmol/L EDTA) without detergents. After centrifugation at 21,000 × *g* for 5 min, the supernatants were further diluted and subjected to sandwich ELISAs for $A\beta_{40}$, $A\beta_{42}$, or sAPPα.

Long-term treatment of Tg2576 by TAK-070

Male and female Tg2576 mice at 7 months of age ($n = 16–17$ for each group, $n = 8–9$, male; $n = 8$, female) were used for long-term treatment with TAK-070. Tg2576 mice were fed chow containing TAK-070 (56 ppm, corresponding to ~7 mg/kg/d, p.o., when evaluated at 6 months of treatment) for 6 months and a week from 7 months of age, or chow without TAK-070 (vehicle control). Male Tg2576 mice at 8 months of age ($n = 9$) were used as a young control. After decapitation, the brains were removed and the left cerebral hemisphere was immediately frozen on dry ice and stored at −80°C until biochemical assays; the right hemisphere was fixed in 4% paraformaldehyde for 24 h, embedded in paraffin, and subjected to immunohistochemical analysis. Biochemical quantitation of Aβ and sAPPα was performed as follows: the cerebral cortex was initially homogenized with ice-cold Tris-extraction buffer and centrifuged as in the short-term treatment study to obtain the supernatants for quantitation of soluble Aβ and sAPPα. The pellet was then homogenized in a 19-fold volume of ice-cold 70% formic acid, and centrifuged at 44,000 × *g* for 5 min. The supernatant was further diluted, neutralized with 1 mol/L Tris-based solution, and the levels of insoluble $A\beta_{40}$ and $A\beta_{42}$ were quantitated by ELISA.

Immunohistochemistry

Immunohistopathological analysis was performed on two distinct coronal sections from the right hemisphere at the level of the hippocampus and thalamus of Tg2576 mice. Sample preparation and quantitation of Aβ plaques were conducted under blinded conditions for the examiner. Four-micrometer-thick sections were deparaffinized and pretreated with 99% formic acid for 5 min. The section was blocked with 10% fetal calf serum for 30 min and then reacted with BAN50 (0.5 μg/ml) at 4°C overnight. BAN50-positive plaques were visualized with Dako REAL EnVision Detection Kit (Dako) using diaminobenzidine as a chromogen. The amyloid burden with a diameter more than ~30 μm (percentage of immunopositive areas that comprised the total area) and the number of plaques throughout the right cerebral neocortices were quantitated using Vanox-(AH-2, Olympus) connected to a digital video camera (Prog Res 3012, Carl Zeiss) and image analysis software (Win ROOF, Mitani).

Y-maze and Morris water maze tests

Male Tg2576 mice of 18 weeks of age were divided into three groups, i.e., vehicle-treated ($n = 14$), TAK-070 1 mg/kg treated ($n = 14$), and TAK-070 3 mg/kg treated ($n = 14$). Wild-type littermates ($n = 15$) were used

as a nontransgenic control group. Tg2576 mice were treated with TAK-070 (1 or 3 mg/kg, p.o.) or vehicle (0.5% methylcellulose; MC) once a day for 9 d before the behavioral test. Each mouse was treated with drugs after all trials were completed every day during the test period. Each mouse was sequentially subjected to Y-maze test on day 10, and then in Morris water maze test from day 11 to day 13. On day 14, the mice were decapitated. The brains were dissected out on ice immediately and stored at −80°C.

Y-maze test. To measure spontaneous alternation behavior and exploratory activity, a black Y-maze with arms of 40 cm length, 3 cm width, with 12.5 cm walls was used. Each animal underwent one trial, during which the animal was placed into one of the three alleys and allowed free exploration of the maze for 5 min, and alternations and total numbers of arm choices were recorded. Spontaneous alternation, expressed as a percentage, refers to ratio of arm choices differing from the previous two choices to the total number of arm entries.

Morris water maze test. The water maze pool comprised a circular plastic water tank, 120 cm in diameter and 20 cm in depth. The pool was filled with water at room temperature to a height of 15 cm. A transparent acrylic platform (10 × 10 cm), its top surface being 0.5 cm below the surface of water, was located in a constant position in the middle of one quadrant from the center and edge of the pool, and was invisible for mice inside the pool. Each mouse was given four trials daily for 3 consecutive days with an interval of ~20 min. The sequence of the starting points was randomly selected. The escape latency and the swimming distance for mice to find the hidden platform were automatically recorded by the computer analyzing system (Target/2, Neuroscience). The value for each session was defined as the mean of four trials. The probe test was not conducted because the deficits were too modest to evaluate the effects of compounds.

Novel object recognition test

Male Tg2576 mice of 5 months of age were divided into two groups, vehicle treated (n = 14) and TAK-070 3 mg/kg treated (n = 15). As a nontransgenic control group, wild-type littermates (n = 15) were used. Tg2576 mice were treated with TAK-070 (3 mg/kg, p.o.) or vehicle (0.5% MC) once a day for 15 d before the test. During the test, each mouse was treated with TAK-070 or vehicle after all trials were completed.

Each mouse was subjected to the novel object recognition test from day 16 to day 17. In the acquisition session on day 16, the same two objects were placed in the back corner of the test box (30 × 30 × 30 cm). The mouse was then placed in another corner of the box and the time exploring each object was recorded for 5 min. After 24 h later on day 17, animals were placed back into the same box, except that one of the familiar objects used during the acquisition was replaced with a novel object. The animals were then allowed to explore freely for 5 min. A preference ratio of the time exploring the novel object to the time exploring both objects was calculated as an index of cognitive function.

Statistical analysis

Statistical analysis was performed by the one-tailed Williams' test for analysis of multiple groups in dose–response study, by Tukey's test for analysis of multiple groups in no dose–response study or Student's t test for analysis of two groups under the BSAS program.

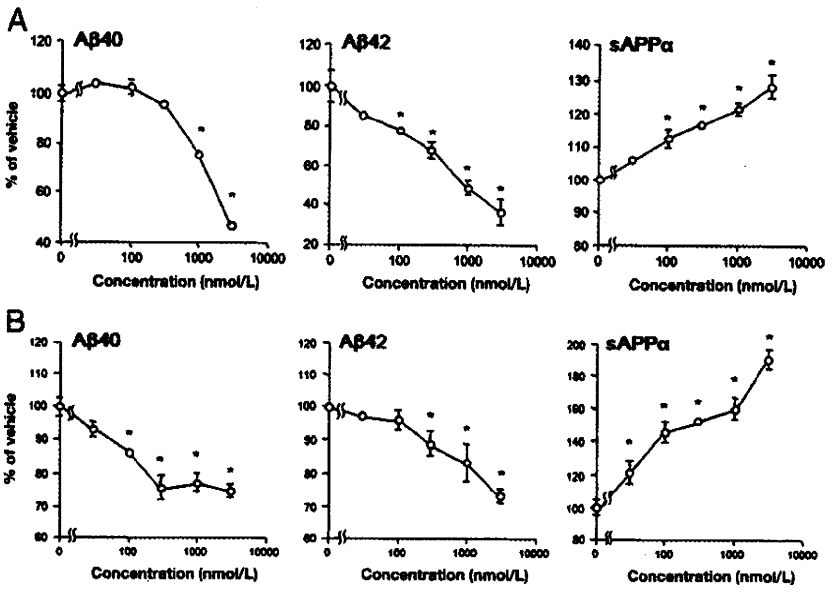

Figure 2. Effects of TAK-070 on secretion of Aβ and sAPPα in cultured cells. The levels of $Aβ_{40}$, $Aβ_{42}$, and sAPPα secreted in conditioned media were quantitated by ELISAs. *A*, Human IMR32 neuroblastoma cells were treated with TAK-070 for 24 h. Vehicle control levels for $Aβ_{40}$ and $Aβ_{42}$ were 17.3 and 5.8 fmol/ml on average, respectively. Levels of sAPPα were determined as arbitrary unit values. Values are mean percentages relative to levels in the control (±SEM) in four independent experiments. *B*, Mouse Neuro2a neuroblastoma cells stably expressing human APPsw (N2aAPPsw cells) were treated with TAK-070 for 24 h. Vehicle control levels of $Aβ_{40}$ and $Aβ_{42}$ were 447.6 and 114.6 fmol/ml, respectively. Levels of sAPPα were determined as arbitrary unit values. Values are mean percentages of the control (±SEM) in six independent experiments. *$p < 0.025$, compared with the vehicle control (one-tailed Williams' test).

Results

TAK-070 reduced Aβ secretion and increased that of sAPPα in cell cultures

We treated human IMR-32 neuroblastoma cells with TAK-070 for 24 h, and measured the levels of Aβ and sAPPα in the conditioned media by ELISA. We observed a concentration-dependent suppression of the secretion of Aβ, with minimum effective concentrations (MECs) for $Aβ_{40}$ and $Aβ_{42}$ of ~100 and ~1000 nmol/L, respectively (Fig. 2*A*). TAK-070 also stimulated sAPPα production in a concentration-dependent manner with MEC of ~100 nmol/L. The percentage reduction in the levels of $Aβ_{40}$ and $Aβ_{42}$, and percentage increase in that of sAPPα by treatment with 3 μmol/L TAK-070 were ~50, ~70, and ~30%, respectively. Similarly significant effects at submicromolar to micromolar ranges of TAK-070 on APP processing (~25% reduction in Aβ secretion and ~90% increase in sAPPα at 3 μmol/L TAK-070) were observed in mouse Neuro-2a neuroblastoma cells stably overexpressing human APP carrying Swedish-type familial Alzheimer mutation (APPsw; N2aAPPsw cells) (Fig. 2*B*).

TAK-070 inhibited BACE1 activity in cultured cells

We next examined the effects of TAK-070 in N2aAPPsw cells by immunoblot analysis. Treatment with TAK-070 (3 μmol/L) significantly decreased the secreted level of both human Swedish sAPPβ and mouse endogenous sAPPβ, N-terminal counterparts of APP generated by BACE1 cleavage, by ~16 and ~19%, respectively. Simultaneously, the levels of human and mouse endogenous sAPPα were increased by ~70% and ~30%, respectively (Fig. 3*A*). We then examined the effects of TAK-070 on the levels of membrane-bound APP and its C-terminal stubs (e.g., C83 and C99), BACE1, and ADAM10 [a neuronal α-secretase candidate (Jorissen et al., 2010)] in lysates of N2aAPPsw cells. TAK-070 decreased the level of C99 by ~15%, in contrast to the prominent

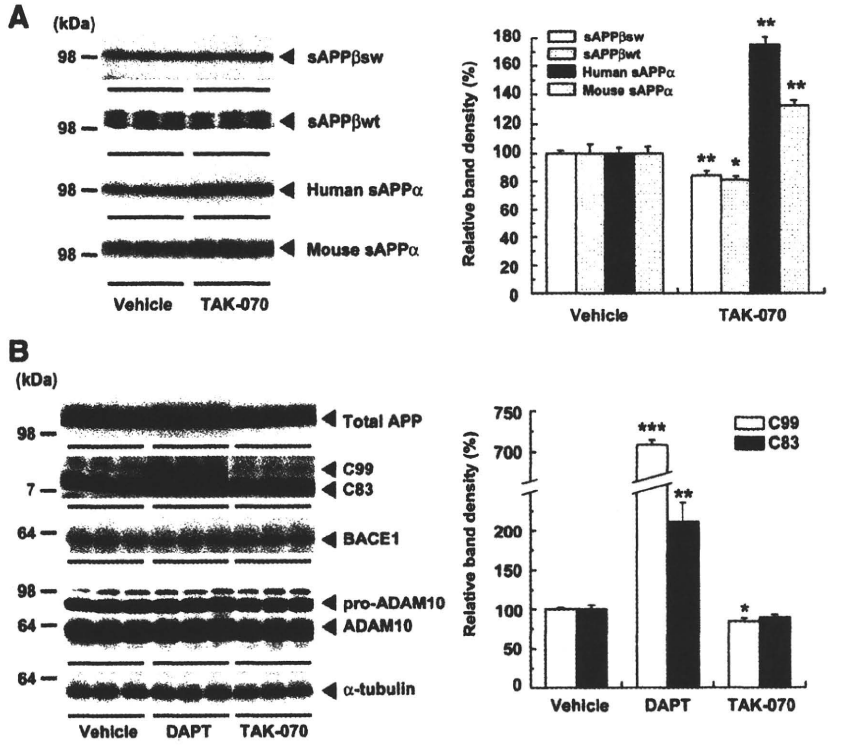

Figure 3. Immunoblot analysis of the protein levels of APP derivatives and those of secretases in N2aAPPsw cells. *A*, Immunoblots of sAPPβ (sAPPβsw derived from transfected human APPsw and sAPPβwt from endogenous mouse APP) and sAPPα (human sAPPα derived from transfected human APPsw and mouse sAPPα from endogenous APP) in media after treatment with TAK-070 (3 μmol/L) or vehicle from three independent experiments are shown. Values in the graph (right) show the mean percentages of band intensities analyzed by densitometry relative to those in vehicle control ($\pm$SEM) in the three independent experiments. $^{*}p < 0.05$, $^{**}p < 0.01$, versus vehicle control (Student's *t* test). *B*, Immunoblots of APP, C-terminal fragments of APP (C99 and C83), BACE1 and high- and low-molecular-weight forms of ADAM10 (pro- and matured forms, respectively) from lysates of N2aAPPsw cells treated with vehicle, DAPT (3 μmol/L), or TAK-070 (3 μmol/L) are shown. Levels of α-tubulin are shown as an internal control. Note that all the immunoblot data are obtained from a single membrane replica with identical exposure. Values for C99 and C83 (right) are mean percentages of band intensities analyzed by densitometry relative to those in vehicle control ($\pm$SEM) in the three independent experiments. $^{*}p < 0.05$, $^{**}p < 0.01$, $^{***}p < 0.001$, versus vehicle control (Student's *t* test).

increase in the levels of C83 and C99 (by ~2.1- and ~7.1-fold, respectively) by inhibition of γ-secretase by DAPT (Fig. 3*B*). TAK-070 treatment did not significantly affect the protein levels of APP, C83, BACE1, or ADAM10 (Fig. 3*B*). The levels of mouse sAPPβ in the conditioned media of TAK-070-treated naive N2a cells also was decreased (supplemental Fig. S1, available at www.jneurosci.org as supplemental material). We further examined the effects of TAK-070 on α-secretase activity using a cell-based, peptide cleavage assay (Doedens et al., 2003). Although (−)-epigallocatechin-3-gallate induced the enzymatic activity, in line with the reported increase in the active form of ADAM10 (Obregon et al., 2006), TAK-070 did not show any incremental effects on the α-secretase-cleaved product (supplemental Fig. S2, available at www.jneurosci.org as supplemental material), suggesting that TAK-070 is not an α-secretase activator.

Noncompetitive BACE1 inhibition by TAK-070 in a cell-free assay

To confirm that TAK-070 has a direct inhibitory effect on BACE1, we developed a cell-free assay, using recombinant full-length human BACE1 and a quenching type fluorogenic BACE1 substrate based on ~10 aa residues flanking the β-cleavage site of wild-type human APP. TAK-070 inhibited the BACE1 activity in a concentration-dependent manner, with IC_{35} of ~3.15 μmol/L and MEC of ~100 nmol/L (Fig. 4*A*), the latter being a similar effective concentration to that in cell culture studies (Fig. 2*A*,*B*). Under the same experimental conditions, a peptidic BACE1 inhibitor (TEEISEVNXVAEF; X = statine) inhibited BACE1 activity with IC_{35} value of 38.8 nmol/L, which was consistent with the previously published data (Sinha et al., 1999). To further examine the inhibitory profile of TAK-070, we conducted a Lineweaver–Burk plot analysis by incubating the fluorogenic BACE1 substrate with recombinant full-length human BACE1 in the presence of 10 or 30 μmol/L TAK-070. All fitted lines converged at an identical point on the *x*-axis with an estimated K_m value of 156 μmol/L (Fig. 4*B*), indicating that TAK-070 inhibits BACE1 in a noncompetitive manner. The K_i value estimated from the *y*-axis values with an intercept of $(1 + [I]/K_i)/V_{max}$ was 19 μmol/L.

TAK-070 did not inhibit other aspartic proteases (e.g., cathepsin D and E, renin, and γ-secretase (Takahashi et al., 2003)), nor activated enzymatic activity of human TACE in cell-free assays even at the concentration of 100 μmol/L (data not shown), in agreement with the cell culture data described above.

Binding of TAK-070 to full-length BACE1, but not to its extracellular domain

To gain further insight into the mechanism of the noncompetitive BACE1 inhibition by TAK-070, we examined the binding of TAK-070 to BACE1 using a surface plasmon resonance assay. Since TAK-070 inhibited the proteolytic activity of full-length BACE1 [BACE1 (1-501)] in a noncompetitive manner, but not that of the truncated BACE1 (1-454), lacking the transmembrane domain (data not shown), we first compared the binding of TAK-070 to BACE1 (1-501) or truncated BACE1 (1-454). Surface Plasmon resonance assay clearly showed that TAK-070 was specifically bound to BACE1 (1-501) in a concentration-dependent manner (0.5–8 μmol/L), but not to BACE1 (1-454) within the same concentration range (Fig. 5*A*). To further narrow down the binding site of TAK-070 within the C-terminal region of BACE1, we examined the binding of TAK-070 to a series of C-terminally truncated BACE1, i.e., BACE1 (1-460), (1-465), (1-471), and (1-474). The binding of TAK-070 to BACE1 (1-460) and (1-465) was completely lost, whereas BACE1 (1-474) retained a comparable affinity to TAK-070 as BACE1 (1-501), and the binding of BACE1 (1-471) was partially impaired (Fig. 5*B*). These data suggest that the critical region within the C terminus of BACE1 for binding to TAK-070 resides around residues 465-474, a subdomain of the membrane spanning region. We also examined the binding of TAK-070 to recombinant proteins of APP (18-688) containing Kunitz-type protease inhibitor domain and the BACE1-cleavage site or sAPPβ, and found that neither APP (18-688) nor sAPPβ showed significant binding to TAK-070 (5

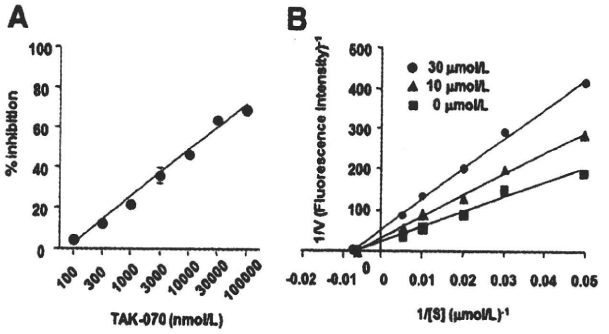

Figure 4. Noncompetitive inhibition of BACE1 activity by TAK-070 in cell-free assay. ***A***, Concentration-dependent inhibition of BACE1 activity by TAK-070. Human recombinant full-length BACE1 purified from COS-7 cells (rhBACE1) was incubated with a fluorogenic BACE1 substrate based on the amino acid sequence of wild-type human APP flanking the BACE1 cleavage site (Nma-SEVKMDAEK(Dnp)RR-NH2) in the presence of various concentrations of TAK-070 (indicated in abscissa, in nanomoles per liter). Values are mean percentage inhibition (± SEM) in three independent experiments. ***B***, Lineweaver–Burk plot analysis of the mode of inhibition by TAK-070. rhBACE1 was incubated with 20–200 μmol/L BACE1 substrate in the presence (10 or 30 μmol/L) or absence of TAK-070. The plots of 1/*V* versus 1/[S] were fitted by the Lineweaver–Burk straight line. Result of a representative experiment is shown.

μmol/L) (supplemental Fig. S3, available at www.jneurosci.org as supplemental material).

These data from cell-based and cell-free studies collectively indicate that TAK-070 is a direct, noncompetitive inhibitor for BACE1 that acts by binding to the noncatalytic site of BACE1, presumably to the transmembrane domain.

TAK-070 reduced Aβ and increased sAPPα in the brains of Tg2576 mice

We then examined whether TAK-070 is effective on Aβ and sAPPα in the brains of Tg2576 mice, a transgenic mouse model of AD that overexpresses APPsw. We first performed a short-term treatment, feeding young female Tg2576 mice with chow containing TAK-070 (5.6 and 56 ppm, corresponding to 0.87 and 8.2 mg/kg/d, p.o., respectively) starting at 2 months of age for 7 weeks. All mice survived without any differences in body weight and food consumption among cohorts. Oral administration of TAK-070 significantly reduced the levels of soluble $A\beta_{40}$ and $A\beta_{42}$ in Tris buffer-soluble fractions of the cerebral cortex (average ± SEM: 7707 ± 334 and 1825 ± 100 fmol/g wet weight, respectively, in vehicle group) by ~16–23%, and increased that of sAPPα by ~15–21% at both doses (Fig. 6*A*).

We next conducted a long-term treatment of Tg2576 mice with TAK-070. We started treatment at the age of ~7 months, just before Tg2576 mice develop the Aβ deposition as amyloid plaques (at ~8 months). Tg2576 mice were fed with chow containing 56 ppm TAK-070 until 13 months of age for ~6 months. Tg2576 mice tolerated chronic treatment with TAK-070, and the mean survival rates were at similar levels after ~6 months treatment by vehicle or TAK-070 (81% or 94%, respectively), without any differences in body weights and food consumption between cohorts.

We first quantitated the levels of Tris-soluble Aβ in the brains of untreated 13-month-old Tg2576 mice, which were dramatically increased by 68% and 129%, respectively for $A\beta_{40}$ and $A\beta_{42}$, compared with those at 8 months (Fig. 6*B*). Notably, the level of sAPPα was decreased by 32% at 13 months. Consistent with the results in young Tg2576 mice (Fig. 6*A*), TAK-070 reduced the levels of Tris-soluble $A\beta_{40}$ and $A\beta_{42}$ by ~15 and ~25%, respectively, and increased that of sAPPα by ~22% even after the 6 months of treatment (Fig. 6*B*).

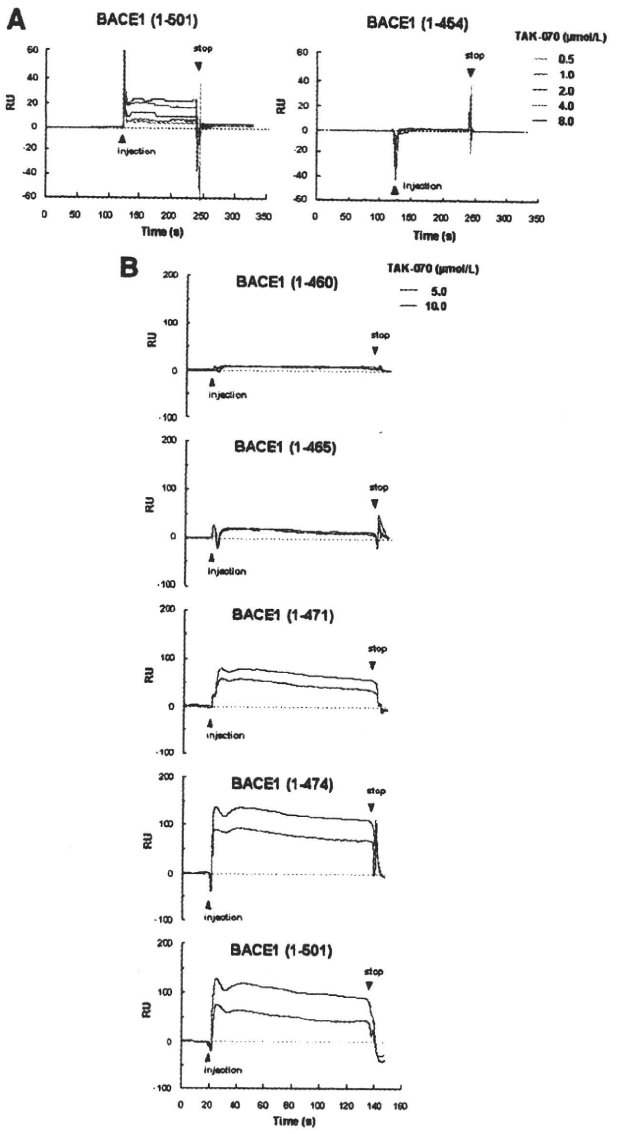

Figure 5. Surface plasmon resonance assay of the binding of TAK-070 to BACE1. ***A***, Sensorgram showing a binding of TAK-070 to full-length BACE1 (1-501) (left panel), but not to C-terminally truncated BACE1 (1-454) lacking the membrane spanning region (right panel). TAK-070 bound to full-length BACE1 in a concentration-dependent manner (within the range of 0.5–8 μmol/L). ***B***, Binding of TAK-070 (5 and 10 μmol/L) to full-length BACE1 (1-501) or C-terminally truncated BACE1 (1-474), (1-471), (1-465), and (1-460). One relative unit (RU) corresponds to 1 pg/mm^2.

We next quantitated the levels of insoluble Aβ that was extracted from the Tris-insoluble pellets by formic acid denaturation. The levels of insoluble $A\beta_{40}$ and $A\beta_{42}$ in untreated Tg2576 mice were markedly increased at 13 months by ~35-fold and ~23-fold, respectively, compared with those of young control mice (6367 ± 720 and 3513 ± 317 pmol/g wet weight, in 8 months of Tg2576). No gender differences were noted in the extent of age-related Aβ increase in our cohort (data not shown). Chronic TAK-070 treatment significantly reduced the levels of insoluble $A\beta_{40}$ and $A\beta_{42}$ by ~30% (Fig. 6*C*).

We then analyzed the effects of TAK-070 on the formation of Aβ plaques using immunohistochemistry and unbiased morphometric analysis. The numbers of Aβ plaques in the cerebral neocortex and hippocampus in TAK-070-treated cohort were markedly reduced

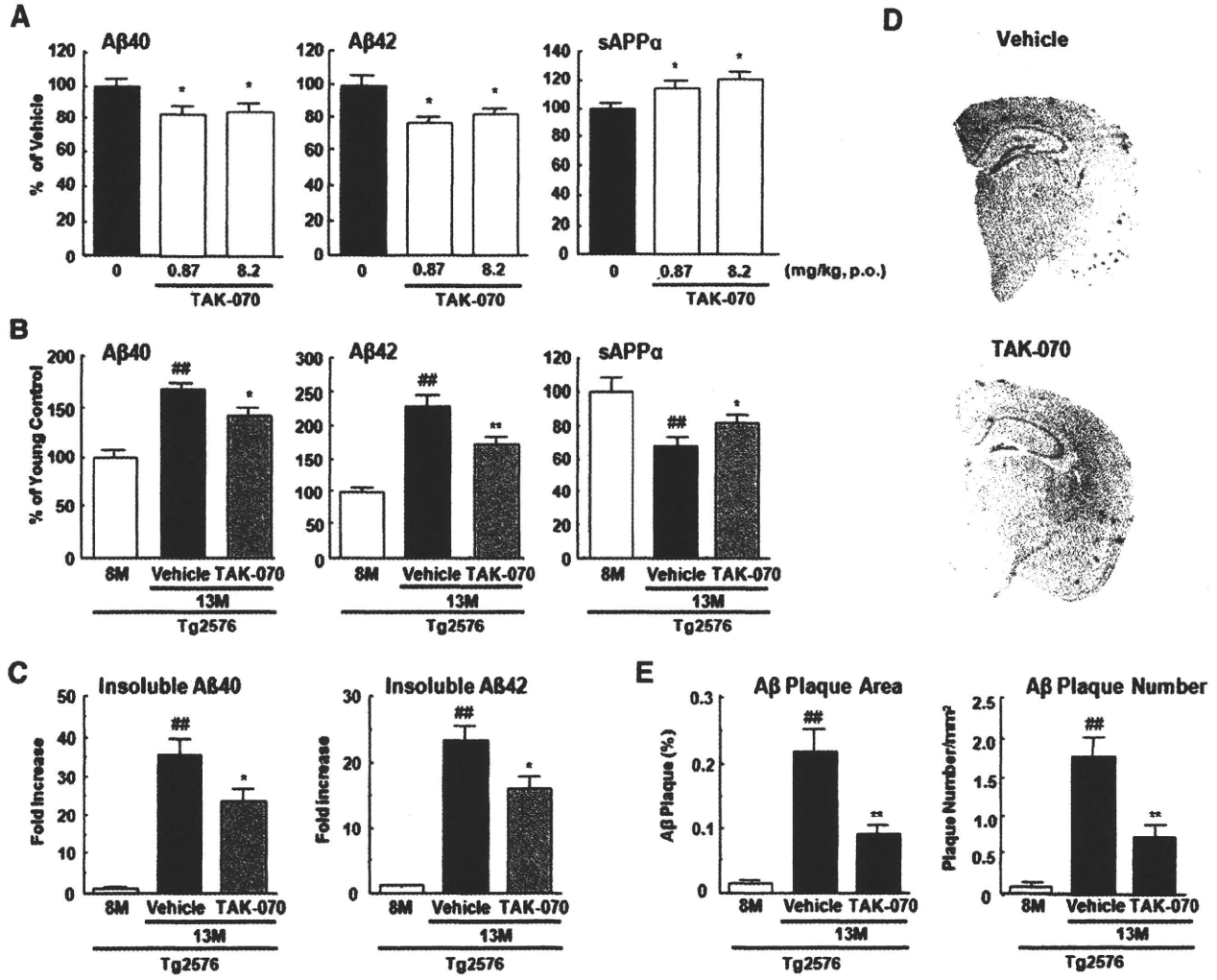

Figure 6. Effects of TAK-070 on Aβ and sAPPα levels in the brains of Tg2576 mice. ***A***, Levels of Tris-soluble $A\beta_{40}$, $A\beta_{42}$, and sAPPα in the cerebral cortices of young female Tg2576 mice after short-term administration. Values are mean percentages (±SEM) relative to levels in vehicle control ($n = 15$ for both cohorts). $^{*}p < 0.025$, versus vehicle control (one-tailed Williams test). ***B***, Levels of Tris-soluble $A\beta_{40}$, $A\beta_{42}$, and sAPPα in cerebral cortices of 13-month-old Tg2576 mice after long-term treatment. The number of 13-month-old Tg2576 mice with vehicle or TAK-070 (56 ppm, corresponding to ~7 mg/kg/d, p.o.) were 13 (male 6, female 7) and 16 (male 10, female 6), respectively after 6 months treatment. Values are mean percentages (±SEM) relative to levels in young controls (8-month-old nontreated Tg2576, $n = 9$). ***C***, Levels of Tris-insoluble, formic acid-extractable $A\beta_{40}$ and $A\beta_{42}$ in cerebral cortices examined in ***B***. Values are the fold increase (±SEM) relative to levels in young controls (8-month-old nontreated Tg2576). ***D***, Aβ immunohistochemistry of coronal sections from brains of TAK-070 (bottom panel) or vehicle (top panel) treated-Tg2576 mice (13 months old). ***E***, Amyloid burden (% of area covered by Aβ immunoreactivity; left panel) or density of plaque (number per mm^2 area; right panel) in the cerebral neocortices of Tg2576 mice. Mean values (±SEM) are shown. $^{\#\#}p < 0.01$, versus those in 8-month-old mice; $^{*}p < 0.05$, $^{**}p < 0.01$, versus those in vehicle control (Student's *t* test) in ***B***, ***C***, and ***E***.

compared to those in the vehicle-treated mice (Fig. 6*D*). Quantitative analysis demonstrated that the Aβ burden (i.e., percentage area covered by Aβ immunoreactivity), as well as the number of plaques per area, were reduced by ~60% upon treatment with TAK-070 (Fig. 6*E*), in agreement with the biochemical data.

TAK-070 ameliorated behavioral deficits in Tg2576 mouse model of AD

We finally assessed the effects of TAK-070 on the behavioral deficits in Tg2576 mice. For this purpose, we conducted three different types of behavioral tests, i.e., Y-maze test, Morris water maze test and a novel object recognition test in relatively young (~5 months old) Tg2576 mice, in which behavioral impairments, along with synaptic deficits, have been documented at this stage, preceding Aβ deposition (Westerman et al., 2002; Ohno et al., 2004; Jacobsen et al., 2006).

We initially conducted Y-maze test, which has been considered as a test for spatial memory. The total arm entries of vehicle-treated Tg2576 mice ($n = 14$) were not significantly different from those of the wild-type control mice ($n = 15$). Treatment with TAK-070 for 9 d did not affect the total arm entries in Tg2576 mice (data not shown), suggesting that repeated treatment with TAK-070 did not have any effects on the basal level of exploring activity. However, the spontaneous alternation in vehicle-treated Tg2576 was significantly reduced to ~50%. This reduction was recovered by treatment with TAK-070 in a dose-dependent manner, and the ameliorating effect was significant at both dosages of 1 ($n = 14$) or 3 mg/kg ($n = 14$) (Fig. 7*A*).

We then assessed the effects of TAK-070 on impairments in spatial memory by sequentially subjecting the same cohorts to the Morris water maze test. The ability of Tg2576 mice to find an invisible platform was impaired compared to that in wild-type mice. On training day 2, significant differences in both escape latency and swimming distance remained between Tg2576 and wild-type mice, whereas they diminished on day 3. Treatment

with TAK-070 reduced the latency (Fig. 7*B*), as well as the distance (Fig. 7*C*), in a dose-dependent manner. On training day 2, the reduction in the swimming distance in TAK-070-treated Tg2576 mice (3 mg/kg) was statistically significant ($p < 0.025$, Williams' test). No significant effects were observed on the swimming speed between the vehicle- and TAK-070-treated mice (data not shown). On the next day of Morris water maze test, we obtained brains from all Tg2576 mice and measured the brain levels of Tris buffer-soluble Aβ peptides, which were decreased by ~9–16% for $A\beta_{40}$, and ~8–12% for $A\beta_{42}$, by administration of 1 and 3 mg/kg TAK-070, respectively, compared with those in vehicle-treated mice. These values were at similar levels to those observed in short-term treatment (see Fig. 6*A*).

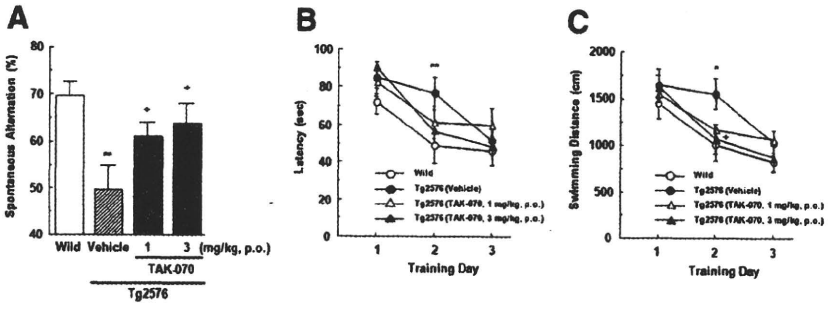

Figure 7. Effects of TAK-070 on impaired behavior of Tg2576 mice in Y-maze test and Morris water maze test. ***A***, Spontaneous alternations (as a percentage) in Y-maze test. ***B***, ***C***, Escape latency (in seconds) (***B***) and swimming distance (in centimeters) (***C***) of mice in the invisible Morris water maze test. Male Tg2576 mice (18 weeks old) were treated with TAK-070 (1 or 3 mg/kg, p.o.) or vehicle for 9 d and then sequentially tested in Y-maze on day 10 and Morris water maze tests on days 11–13. Mean values (±SEM) in 14 animals in each Tg2576 mice group and in 15 wild-type mice (Wild) are shown. $*p < 0.05$, $**p < 0.01$, versus those in Wild (Student's *t* test); $^{+}p < 0.025$, versus those in the vehicle-treated Tg2576 mice (Williams' test).

We further assessed the effects of TAK-070 on recognition memory by a novel object recognition test using new cohorts. After a 15 d successive treatment with vehicle ($n = 15$; wild type mice, $n = 14$; Tg2576) or TAK-070 (3 mg/kg, p.o., $n = 15$; Tg2576), all mice were subjected to an acquisition trial on day 1, in which mice were allowed to get access to the two identical objects in the test box. As expected, all mice equally interacted with both objects in the exploration (data not shown). On the following day, one of the two objects was replaced with a novel one and retention test was conducted. Whereas wild-type mice more frequently interacted with a novel object than a familiar object, with the novel object preference ratio of 78% (Fig. 8*A*,*B*), vehicle-treated Tg2576 mice showed a markedly decreased preference ratio of 44% (Fig. 8*B*), indicating an apparent impairment in recognition memory in Tg2576. By contrast, TAK-070 treatment significantly recovered the preference ratio to a normal range of 71% (Fig. 8*B*).

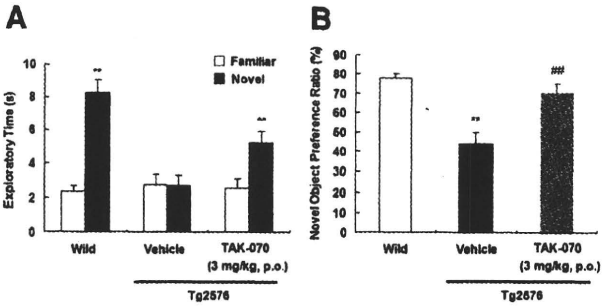

Figure 8. Effects of TAK-070 on impaired behavior of Tg2576 mice in a novel object recognition test. Mean (±SEM) time spent interacting with familiar or novel objects (***A***) and the novel object preference ratio (±SEM) (***B***) in the retention test conducted 24 h after the acquisition trial are shown. ***A***, $**p < 0.01$, versus the familiar control object. ***B***, $**p < 0.01$, versus the wild control, $^{\#\#}p < 0.01$, versus the vehicle-treated control (Student's *t* test).

Discussion

We show that TAK-070 is an orally active BACE1 inhibitor that effectively lowers the levels of soluble Aβ and increases that of sAPPα, inhibits cerebral deposition of insoluble Aβ, and rescues behavioral deficits *in vivo* in a transgenic mouse model of AD. Notably, the partial inhibition in the levels of soluble Aβ eventually resulted in a significant reduction in Aβ deposition after a 6 month chronic treatment, preserving the pharmacological efficacy at a similar level to that in a short-term treatment. We also suggest that TAK-070 exerts a unique noncompetitive inhibitory activity by interacting presumably with the transmembrane region of BACE1 outside the catalytic domain.

Multiple lines of genetic, clinical, and cell biological evidence support the causative role of Aβ in the pathogenesis of AD (for review, see Selkoe and Schenk, 2003). In contrast, sAPPα has been reported to have neurotrophic effects, e.g., promotion of synapse formation or amelioration of cognitive deficits [for review, see Isacson et al. (2002) and Postina (2008)]. In our present study, untreated, aged Tg2576 mice had lower brain levels of sAPPα and higher soluble Aβ with aging, in agreement with previous observations that BACE1 activity is upregulated with aging in the brains of animals as well as humans (Fukumoto et al., 2004; Zohar et al., 2005). Hence, manipulation of APP processing by BACE1 inhibition in a way to reduce Aβ and increase sAPPα would be a rational strategy for the treatment and prevention of AD.

The chemical structure of TAK-070 differs markedly from that of peptide-based BACE1 inhibitors (for review, see Silvestri, 2009). However our cellular and cell-free assay data clearly indicated that TAK-070 is a bona fide BACE1 inhibitor. Cell-free study showed that TAK-070 directly and specifically inhibited full-length BACE1 without affecting other aspartic proteases. TAK-070 reduced levels of secreted Aβ and sAPPβ, together with an increase in sAPPα in cultured cells (Fig. 3), which are in agreement with the previous results of antisense oligonucleotide study for BACE1 (Vassar et al., 1999). The Lineweaver–Burk plot analysis revealed that TAK-070 is a noncompetitive inhibitor (Fig. 4), which was supported by the surface plasmon resonance assay. TAK-070 did bind to the full-length BACE1 (1-501) and truncated BACE1 (1-471 and 474), but not to the truncated BACE1 (1-454, 460, and 465) (Fig. 5). This suggests that TAK-070 inhibits BACE1 activity in a unique mode of interaction by binding to the ~10 aa residues in the C-terminal region (residues 465–474) within the transmembrane domain, but not to the catalytic center (located in residues 93–96 and 289–293). Surface plasmon resonance assay also showed that TAK-070 does not interact with APP(18-688) or sAPPβ (supplemental Fig. S3, available at www.jneurosci.org as supplemental material). This suggests that TAK-070 does not affect APP processing by binding to subdomain of APP containing the BACE1-cleavage sites. We were not able to completely rule out the possibility that TAK-070 interacts with the transmembrane domain of APP, like benzofuran-containing compounds that bind C99 (Espeseth et al., 2005). However, TAK-070 failed to inhibit Aβ secretion from HEK293 cells overexpressing C99 (data not shown), supporting the notion

that TAK-070 does not target C99 in APP. In addition, the possibility that TAK-070 is an α-secretase activator was excluded by (1) the lack of increase in the protein levels of α-secretase candidate, i.e., ADAM10 (Fig. 3), (2) lack of inhibition of TACE activity using a peptidic substrate in a cell-free assay (data not shown), and (3) the lack of increase in α-secretase activity in a cell-based assay (supplemental Fig. S2, available at www.jneurosci.org as supplemental material).

The potency of TAK-070 to reduce the Aβ secretion in cell cultures was modest (i.e., ~25% reduction was achieved at 3 μmol/L with a MEC of ~0.1–0.3 μmol/L in N2aAPPsw cells) (Fig. 2). These results were in agreement with the relatively modest BACE1-inhibitory effect in the cell-free assay with IC_{35} of ~3.15 μmol/L and MEC at ~0.1 μmol/L (Fig. 4). Interestingly, however, we observed similar levels of reduction in soluble Aβ by ~20% in the brains of Tg2576 mice (Fig. 6*A*,*B*). Although small chemicals generally have less potency in brains, hampered by the blood–brain-barrier and cell-penetration issues, this relatively high potency of TAK-070 is likely to be attributable to the highly lipophilic structure bearing *N*-alkyl-amine moiety. In fact, a single administration of TAK-070 in rat (3 mg/kg, p.o.) yielded effective concentration of ~2 μmol/L in brain with the T_{max} of ~24 h using ^{14}C-TAK-070, and the brain exposure levels in short-term- and long-term-treated Tg2576 mice were ~8 μmol/L and ~6–11 μmol/L, respectively (56 ppm of TAK-070, corresponding to ~7–8 mg/kg) (Fig. 6) (our unpublished observations). Furthermore, it has been reported that full-length BACE1, forming a high-molecular-weight complex associated with lipid, exhibits higher enzymatic activity than that of C-terminally truncated BACE1 (1-454) (Marlow et al., 2003; Westmeyer et al., 2004). This may support the view that lipophilic TAK-070 effectively reaches the membrane-associated BACE1 complex.

TAK-070 exhibits ceiling effects on reduction in Aβ and increase in sAPPα (Figs. 2, 6*A*), which may partly be explained by the noncompetitive inhibitory profile for BACE1. We have also observed similar plateau effects in normal rats with a minimum effective dose of 0.1 mg/kg after 4 week administration (our unpublished observation). However, long-term treatment with TAK-070 led to more pronounced Aβ-lowering effects on insoluble Aβ (Fig. 6*C–E*) than on soluble Aβ (Fig. 6*A*,*B*). This finding dovetails with the observation in BACE1 heterozygous KO crossed with PDAPP transgenic mice, in which soluble Aβ levels were lowered only by 12% at a young age, whereas Aβ-accumulation was eventually reduced by ~50–90% with synaptic amelioration in elderly animals (McConlogue et al., 2007). Together, these results strongly suggest that partial inhibition of BACE1, causing partial reduction in Aβ and increase in sAPPα, has sufficient pharmacological efficacy on normalization of APP processing and cognitive functions.

Behavioral deficits in Tg2576 mice have been reported to occur before the deposition of Aβ plaques (Westerman et al., 2002; Ohno et al., 2004; Jacobsen et al., 2006), which may be due to the accumulation of toxic forms of Aβ, e.g., oligomers, that leads to the deterioration of synaptic functions and behaviors (Walsh et al., 2002; Cleary et al., 2005; Venkitaramani et al., 2007). In the present study, relatively young (~5 months) Tg2576 mice showed impairment in behaviors both in Y-maze and novel object recognition tests, whereas the deficits in Morris water maze test were modest, with no differences in the acquisition trial on day 3 between Tg2576 and wild-type cohorts. TAK-070 ameliorated all these behavioral deficits by a short-term treatment at biochemically effective doses (1–3 mg/kg, p.o.) (Figs. 7, 8). TAK-070 had ameliorative effects in the Y-maze and Morris water maze tests that reflect the hippocampal-dependent learning, in line with observations in BACE1 homozygous KO/APP transgenic bigenic mice (Ohno et al., 2004, 2006, 2007). However, there were pivotal differences: TAK-070 treatment affected neither the total number of arm entry in Y-maze test (Ohno et al., 2004) nor the swimming speed in Morris water maze test (Ohno et al., 2006), which were documented to be abnormal in BACE1-homozygous KO regardless of APP-transgenic background. Furthermore, BACE1-homozygous KO in nontransgenic background have been reported to show cognitively deteriorative (Ohno et al., 2004, 2006, 2007), schizophrenia-like (Savonenko et al., 2008), or hypomyelination (Hu et al., 2006; Sankaranarayanan et al., 2008) phenotypes, underscoring the necessity of BACE1 activity for physiological functions, probably due to multiplicity of substrates for BACE1 (for review, see Marks and Berg, 2008). Also in nontransgenic aged rats, TAK-070 ameliorated behavioral deficits in the water maze test (our unpublished observation). Hence, TAK-070 appears to be pharmacologically effective and safe by partial BACE1 inhibition, avoiding adverse events due to complete inhibition of BACE1.

It is noteworthy that the pharmacological effects of orally administered TAK-070 for ~6 months on the brain levels of soluble Aβ and sAPPα were similar to those in short-term treatment (Fig. 6*A*,*B*). Under the chronic treatment, mice were tolerable to TAK-070 and survived comparable to vehicle control after ~6 months. These profiles should be a merit of this compound, considering the long period of AD medication. The sustained efficacy of TAK-070 markedly differs from those documented in other BACE1 inhibitors (Sankaranarayanan et al., 2008) or on the higher efficacy of a compound in the presence of inhibitors of P-glycoprotein (Hussain et al., 2007), that determines exposure levels of compounds in brains.

In sum, the successful treatment by a noncompetitive BACE1 inhibitor, TAK-070, provides strong support for the validity of partial BACE1 inhibition as a disease-modifying as well as symptomatic therapy for AD. TAK-070 will also provide a clue for the elucidation of the mechanism of noncompetitive regulation of the activity of BACE1.

References

Asami-Odaka A, Ishibashi Y, Kikuchi T, Kitada C, Suzuki N (1995) Long amyloid β-protein secreted from wild-type human neuroblastoma IMR-32 cells. Biochemistry 34:10272–10278.

Chen Q, Nakajima A, Choi SH, Xiong X, Tang YP (2008) Loss of presenilin function causes Alzheimer's disease-like neurodegeneration in the mouse. J Neurosci Res 86:1615–1625.

Cleary JP, Walsh DM, Hofmeister JJ, Shankar GM, Kuskowski MA, Selkoe DJ, Ashe KH (2005) Natural oligomers of the amyloid-β protein specifically disrupt cognitive function. Nat Neurosci 8:79–84.

Cole SL, Vassar R (2008) BACE1 structure and function in health and Alzheimer's disease. Curr Alzheimer Res 5:100–120.

Doedens JR, Mahimkar RM, Black RA (2003) TACE/ADAM-17 enzymatic activity is increased in response to cellular stimulation. Biochem Biophys Res Commun 308:331–338.

Donoviel DB, Hadjantonakis AK, Ikeda M, Zheng H, Hyslop PS, Bernstein A (1999) Mice lacking both presenilin genes exhibit early embryonic patterning defects. Genes Dev 13:2801–2810.

Espeseth AS, Xu M, Huang Q, Coburn CA, Jones KLG, Ferrer M, Zuck PD, Strulovici B, Price EA, Wu G, Wolfe AL, Lineberger JE, Sardana M, Tugusheva K, Pietrak BL, Crouthamel M-C, Lai M-T, Dodson EC, Bazzo R, Shi X-P, et al. (2005) Compounds that bind APP and inhibit Aβ processing in vitro suggest a novel approach to Alzheimer disease therapeutics. J Biol Chem 280:17792–17797.

Fukumoto H, Tomita T, Matsunaga H, Ishibashi Y, Saido TC, Iwatsubo T (1999) Primary cultures of neuronal and non-neuronal rat brain cells secrete similar proportions of amyloid β peptides ending at Aβ40 and Aβ42. Neuroreport 10:2965–2969.

Fukumoto H, Rosene DL, Moss MB, Raju S, Hyman BT, Irizarry MC (2004) β-secretase activity increases with aging in human, monkey, and mouse brain. Am J Pathol 164:719–725.

Hu X, Hicks CW, He W, Wong P, Macklin WB, Trapp BD, Yan R (2006) Bace1 modulates myelination in the central and peripheral nervous system. Nat Neurosci 9:1520–1525.

Hussain I, Hawkins J, Harrison D, Hille C, Wayne G, Cutler L, Buck T, Walter D, Demont E, Howes C, Naylor A, Jeffrey P, Gonzalez MI, Dingwall C, Michel A, Redshaw S, Davis JB (2007) Oral administration of a potent and selective non-peptidic BACE-1 inhibitor decreases β-cleavage of amyloid precursor protein and amyloid-β production in vivo. J Neurochem 100:802–809.

Isacson O, Seo H, Lin L, Albeck D, Granholm AC (2002) Alzheimer's disease and Down's syndrome: roles of APP, trophic factors and ACh. Trends Neurosci 25:79–84.

Iwatsubo T, Odaka A, Suzuki N, Mizusawa H, Nukina N, Ihara Y (1994) Visualization of Aβ42(43) and Aβ40 in senile plaques with end-specific Aβ monoclonals: evidence that an initially deposited species is Aβ42(43). Neuron 13:45–53.

Jacobsen JS, Wu CC, Redwine JM, Comery TA, Arias R, Bowlby M, Martone R, Morrison JH, Pangalos MN, Reinhart PH, Bloom FE (2006) Early-onset behavioral and synaptic deficits in a mouse model of Alzheimer's disease. Proc Natl Acad Sci U S A 103:5161–5166.

Jorissen E, Prox J, Bernreuther C, Weber S, Schwanbeck R, Serneels L, Snellinx A, Craessaerts K, Thathiah A, Tesseur I, Bartsch U, Weskamp G, Blobel CP, Glatzel M, De Strooper B, Saftig P (2010) The disintegrin/metalloproteinase ADAM10 is essential for the establishment of the brain cortex. J Neurosci 30:4833–4844.

Lakshmana MK, Yoon IS, Chen E, Bianchi E, Koo EH, Kang DE (2009) Novel role of RanBP9 in BACE1 processing of amyloid precursor protein and amyloid β peptide generation. J Biol Chem 284:11863–11872.

Marks N, Berg MJ (2008) Neurosecretases provide strategies to treat sporadic and familial Alzheimer disorders. Neurochem Int 52:184–215.

Marlow L, Cain M, Pappolla MA, Sambamurti K (2003) β-Secretase processing of the Alzheimer's amyloid protein precursor (APP). J Mol Neurosci 20:233–239.

McConlogue L, Buttini M, Anderson JP, Brigham EF, Chen KS, Freedman SB, Games D, Johnson-Wood K, Lee M, Zeller M, Liu W, Motter R, Sinha S (2007) Partial reduction of BACE1 has dramatic effects on Alzheimer plaque and synaptic pathology in APP transgenic mice. J Biol Chem 282:26326–26334.

Obregon DF, Rezai-Zadeh K, Bai Y, Sun N, Hou H, Ehrhart J, Zeng J, Mori T, Arendash GW, Shytle D, Town T, Tan J (2006) ADAM10 activation is required for green tea (-)-epigallocatechin-3-gallate-induced (alpha)-secretase cleavage of amyloid precursor protein. J Biol Chem 281:16419–16427.

Ohno M, Sametsky EA, Younkin LH, Oakley H, Younkin SG, Citron M, Vassar R, Disterhoft JF (2004) BACE1 deficiency rescues memory deficits and cholinergic dysfunction in a mouse model of Alzheimer's disease. Neuron 41:27–33.

Ohno M, Chang L, Tseng W, Oakley H, Citron M, Klein WL, Vassar R, Disterhoft JF (2006) Temporal memory deficits in Alzheimer's mouse models: rescue by genetic deletion of BACE1. Eur J Neurosci 23:251–260.

Ohno M, Cole SL, Yasvoina M, Zhao J, Citron M, Berry R, Disterhoft JF, Vassar R (2007) BACE1 gene deletion prevents neuron loss and memory deficits in 5XFAD APP/PS1 transgenic mice. Neurobiol Dis 26:134–145.

Postina R (2008) A closer look at α-secretase. Curr Alzheimer Res 5:179–186.

Sankaranarayanan S, Price EA, Wu G, Crouthamel MC, Shi XP, Tugusheva K, Tyler KX, Kahana J, Ellis J, Jin L, Steele T, Stachel S, Coburn C, Simon AJ (2008) In vivo beta-secretase 1 inhibition leads to brain Aβ lowering and increased α-secretase processing of amyloid precursor protein without effect on neuregulin-1. J Pharmacol Exp Ther 324:957–969.

Sankaranarayanan S, Holahan MA, Colussi D, Crouthamel MC, Devanarayan V, Ellis J, Espeseth A, Gates AT, Graham SL, Gregro AR, Hazuda D, Hochman JH, Holloway K, Jin L, Kahana J, Lai MT, Lineberger J, McGaughey G, Moore KP, Nantermet P, et al. (2009) First demonstration of cerebrospinal fluid and plasma Aβ lowering with oral administration of a β-site amyloid precursor protein-cleaving enzyme 1 inhibitor in nonhuman primates. J Pharmacol Exp Ther 328:131–140.

Saura CA, Choi SY, Beglopoulos V, Malkani S, Zhang D, Shankaranarayana Rao BS, Chattarji S, Kelleher RJ 3rd, Kandel ER, Duff K, Kirkwood A, Shen J (2004) Loss of presenilin function causes impairments of memory and synaptic plasticity followed by age-dependent neurodegeneration. Neuron 42:23–36.

Saura CA, Chen G, Malkani S, Choi SY, Takahashi RH, Zhang D, Gouras GK, Kirkwood A, Morris RG, Shen J (2005) Conditional inactivation of presenilin 1 prevents amyloid accumulation and temporarily rescues contextual and spatial working memory impairments in amyloid precursor protein transgenic mice. J Neurosci 25:6755–6764.

Savonenko AV, Melnikova T, Laird FM, Stewart KA, Price DL, Wong PC (2008) Alteration of BACE1-dependent NRG1/ErbB4 signaling and schizophrenia-like phenotypes in BACE1-null mice. Proc Natl Acad Sci U S A 105:5585–5590.

Selkoe DJ, Schenk D (2003) Alzheimer's disease: molecular understanding predicts amyloid-based therapeutics. Annu Rev Pharmacol Toxicol 43:545–584.

Shen J, Bronson RT, Chen DF, Xia W, Selkoe DJ, Tonegawa S (1997) Skeletal and CNS defects in Presenilin-1-deficient mice. Cell 89:629–639.

Silvestri R (2009) Boom in the development of non-peptidic β-secretase (BACE1) inhibitors for the treatment of Alzheimer's disease. Med Res Rev 29:295–338.

Sinha S, Anderson JP, Barbour R, Basi GS, Caccavello R, Davis D, Doan M, Dovey HF, Frigon N, Hong J, Jacobson-Croak K, Jewett N, Keim P, Knops J, Lieberburg I, Power M, Tan H, Tatsuno G, Tung J, Schenk D, et al. (1999) Purification and cloning of amyloid precursor protein β-secretase from human brain. Nature 402:537–540.

Stockley JH, O'Neill C (2007) The proteins BACE1 and BACE2 and β-secretase activity in normal and Alzheimer's disease brain. Biochem Soc Trans 35:574–576.

Takahashi Y, Hayashi I, Tominari Y, Rikimaru K, Morohashi Y, Kan T, Natsugari H, Fukuyama T, Tomita T, Iwatsubo T (2003) Sulindac sulfide is a noncompetitive γ-secretase inhibitor that preferentially reduces Aβ42 generation. J Biol Chem 278:18664–18670.

Tomita T, Katayama R, Takikawa R, Iwatsubo T (2002) Complex N-glycosylated form of nicastrin is stabilized and selectively bound to presenilin fragments. FEBS Lett 520:117–121.

Vassar R, Bennett BD, Babu-Khan S, Kahn S, Mendiaz EA, Denis P, Teplow DB, Ross S, Amarante P, Loeloff R, Luo Y, Fisher S, Fuller J, Edenson S, Lile J, Jarosinski MA, Biere AL, Curran E, Burgess T, Louis JC, et al. (1999) β-secretase cleavage of Alzheimer's amyloid precursor protein by the transmembrane aspartic protease BACE. Science 286:735–741.

Venkitaramani DV, Chin J, Netzer WJ, Gouras GK, Lesne S, Malinow R, Lombroso PJ (2007) β-Amyloid modulation of synaptic transmission and plasticity. J Neurosci 27:11832–11837.

Walsh DM, Klyubin I, Fadeeva JV, Cullen WK, Anwyl R, Wolfe MS, Rowan MJ, Selkoe DJ (2002) Naturally secreted oligomers of amyloid beta protein potently inhibit hippocampal long-term potentiation in vivo. Nature 416:535–539.

Westerman MA, Cooper-Blacketer D, Mariash A, Kotilinek L, Kawarabayashi T, Younkin LH, Carlson GA, Younkin SG, Ashe KH (2002) The relationship between Aβ and memory in the Tg2576 mouse model of Alzheimer's disease. J Neurosci 22:1858–1867.

Westmeyer GG, Willem M, Lichtenthaler SF, Lurman G, Multhaup G, Assfalg-Machleidt I, Reiss K, Saftig P, Haass C (2004) Dimerization of β-site β-amyloid precursor protein-cleaving enzyme. J Biol Chem 279:53205–53212.

Wong PC, Zheng H, Chen H, Becher MW, Sirinathsinghji DJ, Trumbauer ME, Chen HY, Price DL, Van der Ploeg LH, Sisodia SS (1997) Presenilin 1 is required for Notch1 and DII1 expression in the paraxial mesoderm. Nature 387:288–292.

Zohar O, Pick CG, Cavallaro S, Chapman J, Katzav A, Milman A, Alkon DL (2005) Age-dependent differential expression of BACE splice variants in brain regions of tg2576 mice. Neurobiol Aging 26:1167–1175.

Neurobiology of Disease

Participation of Transmembrane Domain 1 of Presenilin 1 in the Catalytic Pore Structure of the γ-Secretase

Shizuka Takagi (高木穏香),[1] Aya Tominaga (富永綾),[1] Chihiro Sato (佐藤千尋),[1,2,3] Taisuke Tomita (富田泰輔),[1,2] and Takeshi Iwatsubo (岩坪威)[1,2,3]

[1]Department of Neuropathology and Neuroscience, Graduate School of Pharmaceutical Sciences, The University of Tokyo, Tokyo 113-0033, Japan, [2]Core Research for Evolutional Science and Technology, Japan Science and Technology Corporation, and [3]Department of Neuropathology, Graduate School of Medicine, The University of Tokyo, Hongo 7-3-1, Bunkyo, Tokyo 113-0033, Japan

γ-Secretase is an intramembrane-cleaving protease that is responsible for the generation of amyloid-β peptides linked to the pathogenesis of Alzheimer's disease. Using a substituted cysteine accessibility method, we have previously shown that the hydrophilic "catalytic pore" structure of γ-secretase is formed by the transmembrane domains (TMDs) 6, 7, and 9 of presenilin 1 (PS1), the catalytic subunit of γ-secretase, within the membrane. Here, we analyzed the structure in and around the first hydrophobic region, the putative TMD1, of PS1, of which the precise function as well as three-dimensional location within γ-secretase remained unknown. We found that TMD1 is located in proximity to the catalytic GxGD and PAL motifs within the C-terminal fragment of PS1, facing directly the catalytic pore. Competition experiments using known γ-secretase inhibitors suggested that the N-terminal region of TMD1 functions as a subsite during proteolytic action of the γ-secretase. Intriguingly, binding of inhibitors affected water accessibility of residues at the membrane border of TMD1, suggesting the possibility of a dynamic motion of TMD1 during the catalytic process. Our results provide mechanistic insights into the functional role of TMD1 of PS1 in the intramembrane-cleaving activity of the γ-secretase.

Introduction

The process of generation and deposition of amyloid-β peptide (Aβ) is strongly implicated in the pathogenesis of Alzheimer/s disease (AD) (Haass and Selkoe, 2007). Accordingly, γ-secretase, a protease responsible for the Aβ generation, is one of the plausible therapeutic targets for AD (Tomita, 2009; De Strooper et al., 2010). However, γ-secretase cleaves several type I single-span membrane proteins, including Notch receptor. Thus, the mechanism-based rational design of γ-secretase inhibitors (GSIs) based on the structural information of the γ-secretase is unequivocally needed for development of AD therapeutics. γ-Secretase is an unconventional aspartyl protease that hydrolyzes its substrates within the hydrophobic lipid bilayer. It belongs to a unique group of intramembrane-cleaving proteases (I-CLiPs), of which site 2 protease (S2P), signal peptide peptidase, and rhomboid have been identified as other members (Wolfe and Kopan, 2004). The recently resolved crystal structures of the rhomboid and S2P have shed light on the possible mechanism as to how peptide bond hydrolysis can take place within the lipid environment (Urban and Shi, 2008). Nonetheless, structural analysis such as x-ray crystallography is still an extremely challenging task for multimeric membrane protein complexes (e.g., the γ-secretase), which is comprised of nicastrin, anterior pharynx defective-1, presenilin enhancer-2, and PS (Takasugi et al., 2003). We have been applying substituted cysteine accessibility method (SCAM) to gain insights into the structure of presenilin 1 (PS1) in a membrane-embedded state. SCAM has been reiteratively used to obtain structural information of various multipass membrane proteins in a functional state, by covalently modifying the introduced cysteine (Cys) residues using sulfhydryl reagents (Karlin and Akabas, 1998; Kaback et al., 2001). Using SCAM, we and others have revealed that PS1 harbors a hydrophilic "catalytic pore" formed by transmembrane domains (TMDs) 6, 7, and 9 (Sato et al., 2006, 2008; Tolia et al., 2006, 2008). Recent nuclear magnetic resonance analysis of the C-terminal region of PS1 supported the results of SCAM analysis (Sobhanifar et al., 2010). This was consistent with the structures obtained from the crystallographic analyses of rhomboid and S2P, further suggesting that the hydrophilic milieu around the active site located within the lipid bilayer is a common structure across I-CLiPs. Meanwhile, recent chemical biological studies revealed that several GSIs directly target the N-terminal fragment (NTF) of PS1 (Fuwa et al., 2007; Imamura et al., 2009). Thus, an important remaining question regarding the structure–function relationship of γ-secretase is how the other five TMDs within the PS1 NTF contribute to the γ-secretase activity. Here, we used

Received June 26, 2010; revised Sept. 12, 2010; accepted Sept. 23, 2010.

This work was supported by Grants-in-Aid for Young Scientists (S) (to T.T.) from the Ministry of Education, Culture, Sports, Science, and Technology of Japan (MEXT), by Scientific Research on Priority Areas "Research on Pathomechanisms of Brain Disorders" from MEXT (to T.T., T.I.), by the Program for Promotion of Fundamental Studies in Health Sciences of the National Institute of Biomedical Innovation (to T.T., T.I.), by Targeted Proteins Research Program of the Japan Science and Technology Corporation (JST) (to T.T., T.I.), and by Core Research for Evolutional Science and Technology of JST (to T.T., T.I.), Japan. S.T. and C.S. are research fellows of the Japan Society for the Promotion of Science. We thank Drs. G. Thinakaran (University of Chicago, Chicago, IL) for antibodies, B. De Strooper (KU Leuven, Leuven, Belgium) for DKO cells, T. Kitamura (University of Tokyo, Tokyo, Japan) for retroviral infection system, and Takeda Pharmaceutical Company for Aβ ELISA. We are also grateful to our laboratory members for helpful discussions and technical assistance.

Correspondence should be addressed to Dr. Taisuke Tomita, Department of Neuropathology and Neuroscience, Graduate School of Pharmaceutical Sciences, The University of Tokyo, 7-3-1 Hongo, Bunkyo-ku, Tokyo 113-0033, Japan. E-mail: taisuke@mol.f.u-tokyo.ac.jp.

DOI:10.1523/JNEUROSCI.3318-10.2010

 0270-6474/10/3015943-08$15.00/0

SCAM and other biochemical methods to analyze the structure and the functional role of TMD1 of PS1, which has been shown to be indispensable for the stability, as well as the catalytic activity, of the γ-secretase (Watanabe et al., 2005, 2010).

Materials and Methods

G1L3, which recognizes the hydrophilic loop 6 of PS1, was described previously (Tomita et al., 1999). Anti-$PS1_{NT}$ (Thinakaran et al., 1998) was kindly provided by Dr. Thinakaran (University of Chicago, Chicago, IL). Other antibodies were purchased from BD Biosciences (anti-E-cadherin), Cell Signaling Technology [anti-cleaved Notch1 (V1744) and anti-myc tag (9B11)], or Sigma [anti-α-tubulin (DM1A)]. {1*S*-Benzyl-4*R*-[1-(1*S*-carbamoyl-2-phenylethylcarbamoyl)-1*S*-3-methyl-butylcarbamoyl]-2*R*-hydroxy-5-phenylpentyl}carbamic acid *tert*-butyl ester (L-685,458) (Shearman et al., 2000) and peptide 15 (pep15) (Das et al., 2003) were purchased from Bachem and BEX, respectively. *N*-[*N*-(3,5-difluorophenacetyl)]-*L*-alanyl]-*S*-phenylglycine *tert*-butyl ester (DAPT) was synthesized as described previously (Dovey et al., 2001; Kan et al., 2004). All 3-(4,5-dimethylthiazol-2-yl)-5-(3-carboxymethoxyphenyl)-2-(4-sulfophenyl)-2*H*-tetrazolium (MTS) reagents (Toronto Research Chemicals) were dissolved in DMSO at 200 mM and stored at −80°C until use. The abbreviations used for MTS cross-linkers are described previously (Sato et al., 2006, 2008). cDNAs encoding APP_{NL}, NotchΔE, PS1, and Cysless PS1 [PS1/Cys(−)] were described previously (Kopan et al., 1996; Tomita et al., 1997; Sato et al., 2006). Single- or double-Cys mutant (mt) PS1 cDNAs were generated using a long PCR-based protocol. Maintenance of embryonic fibroblasts derived from *Psen1/Psen2* double knock-out (DKO) cells (Herreman et al., 2000), a retroviral infection system (Kitamura et al., 2003), and generation of stable infectants was performed as described previously (Watanabe et al., 2005, 2010; Sato et al., 2006, 2008). Microsome preparation and immunoblot analysis were performed as described previously (Tomita et al., 1997, 1999, 2001; Takahashi et al., 2003; Hayashi et al., 2004). For the measurement of secreted Aβ, recombinant retrovirus encoding each Cys mt PS1 was transiently infected into DKO cells that stably expressing APP_{NL} (Watanabe et al., 2005). After 24 h incubation, the conditioned medium was collected and subjected to two-site ELISAs (i.e., BAN50/BA27 and BAN50/BC05 for Aβ40 and Aβ42, respectively) (Iwatsubo et al., 1994, Tomita et al., 1997, 1998, 2001). Biotinylation and competition experiments using *N*-biotinylaminoethyl methanethiosulfonate (MTSEA-biotin) in intact cells or microsome fraction have been described in detail before (Sato et al., 2006, 2008; Isoo et al., 2007). Cross-linking experiments were performed as previously described except that the microsomes were prepared from 10 cm dishes per single analysis. For a competition assay, sodium 2-sulfonatoethyl methanethiosulfonate (MTSES), 2-(trimethylammonium)ethyl methanethiosulfonate bromide (MSTET), or 2-(triethylammonium)ethyl methanethiosulfonate (MTS-TEAE) was preincubated with intact cells or microsomes at 2 mM for 5 min at 4°C and washed once before biotinylation. GSIs were preincubated with microsome aliquots for 30 min at room temperature before incubation with cross-linkers. The inhibitors were used at concentrations (L-685,458, 1 μM; DAPT, 10 μM; pep15, 1 μM) that completely abolish the proteolytic activity of γ-secretase (Morohashi et al., 2006; Sato et al., 2006).

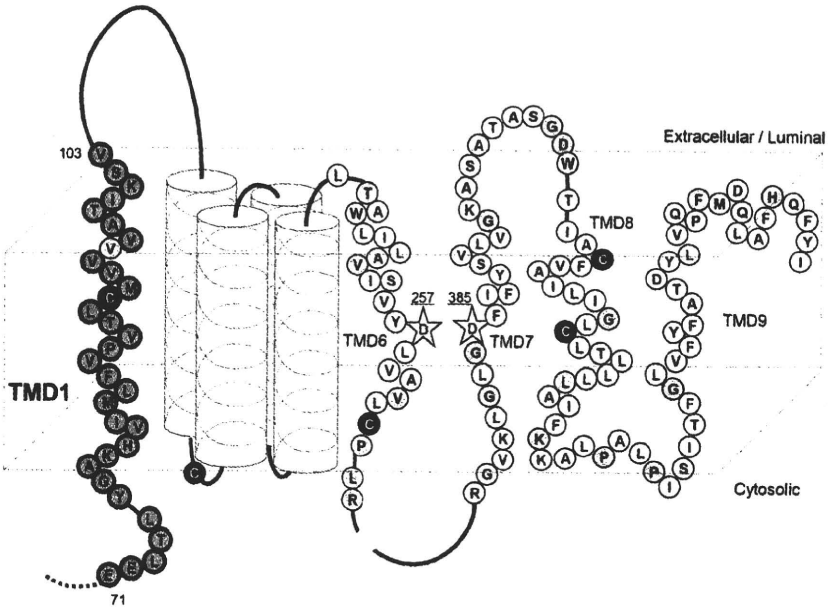

Figure 1. Locations of the PS1 cysteine mutations used in this study. Schematic depiction of human PS1 is shown. Endogenous Cys residues that were replaced with serine in PS1/Cys(−) are indicated as black circles. Amino acid residues substituted to Cys in the present and previous studies are shown by circles with a single-letter character representing the original amino acids. Residues analyzed in this study are indicated by orange circles. Residues in which Cys substitution caused a loss of γ-secretase activity are indicated as gray circles. Catalytic aspartates are shown by yellow stars.

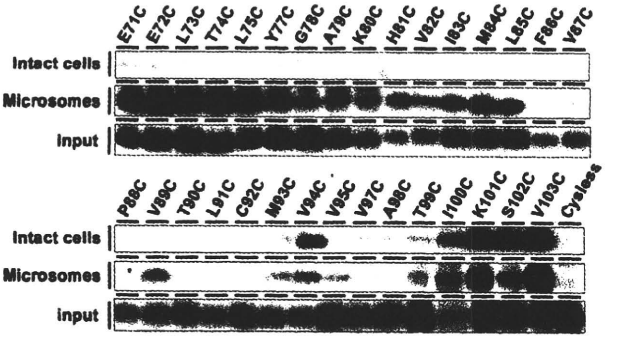

Figure 2. SCAM analysis of single-Cys mt PS1 around HR1. Intact cells (top) expressing single-Cys mt PS1 or the microsomes (middle) were incubated with MTSEA-biotin. Biotinylated proteins were precipitated with streptavidin beads and then subjected to immunoblot analysis. Cysless serves as the negative control. Amount of PS1 NTF in the input fraction is shown in the bottom panel.

Results

SCAM analysis of the hydrophobic region 1 of PS1

Previous computational predictions and cell-based topological studies indicated that the hydrophobic region (HR) 1 of PS1 spans the membrane as TMD1 (Doan et al., 1996; Li and Greenwald, 1996; Lehmann et al., 1997; Nakai et al., 1999). To examine whether this region penetrates the membrane as a TMD and faces to the aqueous environment in the lipid bilayer, we constructed mutant PS1 having a single cysteine residue based on PS1/Cys(−) (single-Cys mt PS1) at 32 different amino acid residues in and around the HR1 (E71-V103), and expressed them in DKO cells (Fig. 1). We excluded V96C from further analyses, because Cys substitution of V96 resulted in loss of expression of PS1 polypeptide and failure in the restoration of the γ-secretase activity (supplemental Fig. 1, available at www.jneurosci.org as supplemental material). All the other single-Cys mt PS1 retained the protein expression, endoproteolysis, and the γ-secretase activity. SCAM analysis of the single-Cys mt PS1 in intact cells revealed that V94C, I100C, K101C, S102C, and V103C were biotinylated by MTSEA-biotin (Fig. 2, top), suggesting that these labeled residues are located in a hydrophilic milieu accessible from the extracel-

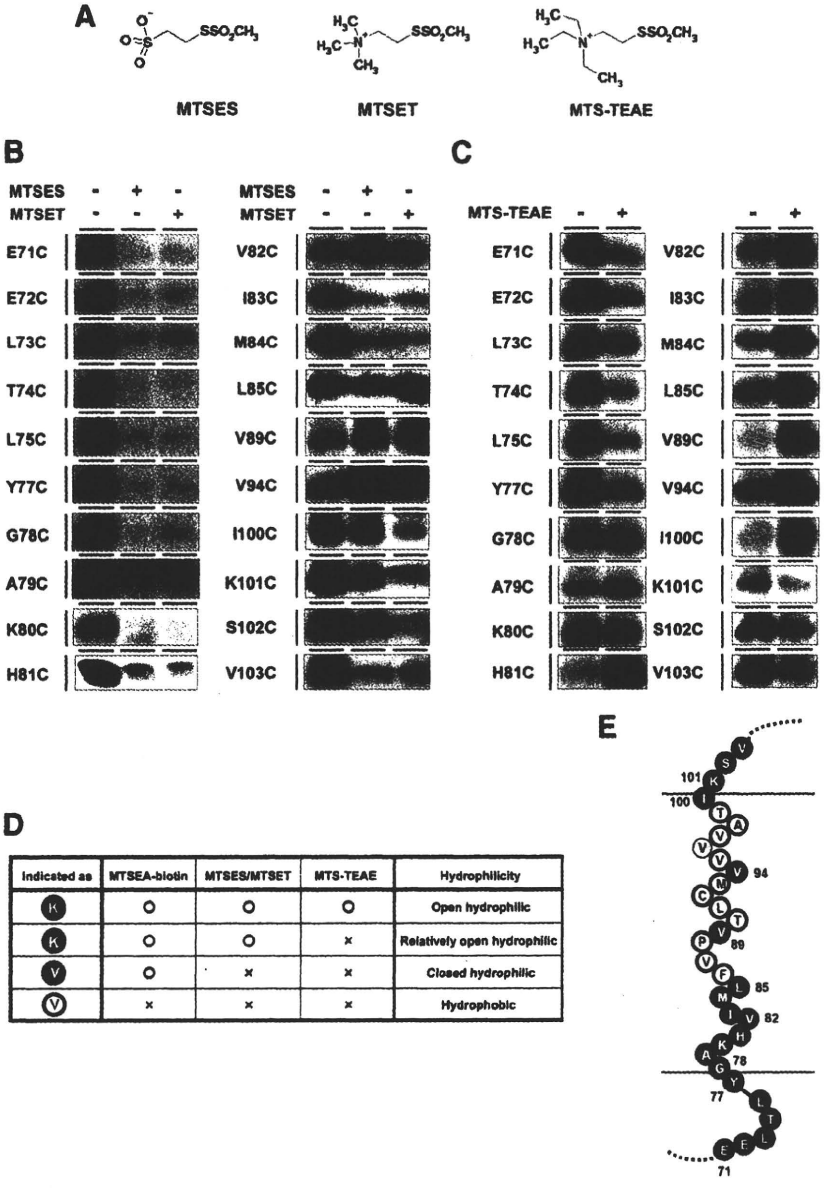

Indicated as	MTSEA-biotin	MTSES/MTSET	MTS-TEAE	Hydrophilicity
K	○	○	○	Open hydrophilic
K	○	○	×	Relatively open hydrophilic
V	○	×	×	Closed hydrophilic
V	×	×	×	Hydrophobic

Figure 3. SCAM analysis of single-Cys mt PS1 using charged MTS reagents. ***A***, The structures of the charged MTS reagents. The abbreviations are indicated below in ***B***. ***B***, Labeling competition of single-Cys mt PS1 around HR1 was examined after preincubation with negatively charged MTSES or positively charged MTSET. ***C***, Labeling competition experiments using positively charged MTS-TEAE with a bulkier structure. ***D***, Summary of the competition experiments using charged MTS reagents. ***E***, Schematic depiction of TMD1. All charged reagents were accessible to the Cys-substituted residues indicated by blue circles. Residues whose labeling was competed by MTSES or MTSET, but not by MTS-TEAE, are indicated by sky-blue circles. Residues whose labeling was not decreased by any charged reagents are indicated by purple circles. Residues that were not labeled by MTSEA-biotin or unanalyzed are shown by black letters in white and gray circles, respectively. The predicted lipid–water interface is indicated by green lines.

Table 1. The summary of the cross-linking experiments in this study

	MTS cross-linkers		
	M84C	V89C	V94C
L383C at GxGD motif	M2M (<5.2 Å)	M2M (<5.2 Å)	M8M (<13.0 Å)
I387C	M8M (<13.0 Å)	M8M (<13.0 Å)	Not cross-linked
L435C at PAL motif	M11M (<16.9 Å)	M2M (<5.2 Å)	ND

"MTS cross-linkers" indicates the abbreviated name of the shortest cross-linker that enabled the production of an NTF-CTF heterodimer (i.e., M2M). Values in parentheses indicate the length of the spacer arm of the MTS cross-linkers. ND, Not determined.

lular side. We next examined the accessibility of MTSEA-biotin to these residues from either the extracellular/luminal or cytosolic sides using microsome fractions from DKO cells expressing single-Cys mt PS1, which have been shown to be composed of a mixture of inside-out and outside-out vesicles (Sato et al., 2006). In addition to the residues that were biotinylated in intact cells, consecutive amino acid residues from E71C to L85C, as well as V89C, were positively labeled with MTSEA-biotin (Fig. 2, middle). The densitometric quantitation of each band is shown in supplemental Figure 2 (available at www.jneurosci.org as supplemental material). These results are consistent with the view that HR1 region spans the lipid bilayer with a type II orientation. Next, we analyzed the steric and electrostatic environment around the water-accessible residues using other membrane-impermeable MTS derivatives (i.e., the negatively charged MTSES and positively charged MTSET) as competitors for MTSEA-biotin (Fig. 3*A*, left and middle) (Sato et al., 2006, 2008). Preincubation with MTSES or MTSET failed to decrease the labeling of V82C, L85C, V89C, and V94C by MTSEA-biotin, whereas the biotinylation of other mutants was abolished by both of the charged MTS reagents (Fig. 3*B*). These data suggest that V82, L85, V89, and V94 are located in a closed hydrophilic environment with limited access to outside within the lipid bilayer. In contrast, other residues in which MTSES and MTSET competed for biotinylation were predicted to be facing an open hydrophilic environment. To further analyze the open hydrophilic environment in detail, we used MTS-TEAE, a sterically bulkier derivative of MTSET (Fig. 3*A*, right). As expected, preincubation with MTS-TEAE did not compete for the biotinylation of the Cys residues to which MTSES or MTSET was inaccessible (i.e., V82C, L85C, V89C, or V94C). However, MTS-TEAE failed to decrease the labeling of G78C, A79C, K80C, H81C, I83C, M84C, and I100C, although the biotinylation of these mutants was competed for that by MTSES or MTSET, suggesting that these residues are located within a relatively open, but sterically hindered, hydrophilic environment. In contrast, the labeling of other mutants (i.e., from E71C through Y77C and K101 through V103C) was decreased by preincubation with MTS-TEAE (Fig. 3*C*). These data indicate that the residues from E71 to Y77 and K101 to V103 are exposed to an open hydrophilic environment with unlimited access at the cytosolic and extracellular sides, respectively (for a summary, see Fig. 3*D*,*E*). Strong labeling of these residues by MTSEA-biotin also supports this notion (Fig. 2; supplemental Fig. 2, available at www.jneurosci.org as supplemental material). Intriguingly, the

biotinylation of some residues was dramatically augmented by preincubation with the membrane-impermeable MTS derivatives, presumably due to the increased availability of MTSEA-biotin by masking of the cysteines of other proteins. Together, these results suggest that the subregion of PS1 from G78 through I100 penetrates the membrane as TMD1, and that the N-terminal region of TMD1 sits in a hydrophilic, but sterically hindered, environment.

Cross-linking experiments using MTS cross-linkers

We have previously shown that the amino acid residues in TMD6 are located in proximity to those in TMD7 and TMD9, which are collectively involved in the formation of the catalytic pore, by cross-linking experiments (Sato et al., 2006, 2008). To investigate whether TMD1 also is facing to the catalytic pore, we performed cross-linking experiments using MTS cross-linkers. M2M, M3M, M4M, M6M, M8M, M11M, M14M, and M17M are sulfhydryl-to-sulfhydryl cross-linking reagents with spacer arms 5.2, 6.5, 7.8, 10.4, 13.0, 16.9, 20.8, and 24.7 Å long, respectively (Loo and Clarke, 2001). No cross-linked products were observed by coincubation with any MTS cross-linker in samples from cells expressing single-Cys mt PS1 (supplemental Fig. 3, available at www.jneurosci.org as supplemental material), in accordance with previous findings (Sato et al., 2006, 2008). We next generated double-Cys mutant PS1 bearing a pair of Cys, one located within TMD1 (M84C, V89C, or V94C) and the other in CTF, in positions previously shown to be located within the catalytic pore (i.e., L383C in TMD7, I387C, and L435C in PAL motif at TMD9) (for a summary, see Table 1). All double-Cys mt PS1 showed the γ-secretase activity (supplemental Fig. 4, available at www.jneurosci.org as supplemental material). Coincubation of all double-Cys mt PS1 (except V94C/I387C) with MTS cross-linkers yielded a novel band migrating closely to the PS1 holoprotein (Fig. 4; supplemental Fig. 5, available at www.jneurosci.org as supplemental material). Anti-PS1 NTF and CTF antibodies gave the same results, suggesting that these bands correspond to cross-linked products of NTF and CTF of PS1, in accordance with the previous observations (Sato et al., 2006, 2008). These results indicate that TMD1 faces an identical hydrophilic catalytic pore that is formed by TMD7 and TMD9. Notably, in M84C/L383C, V89C/L383C, and V89C/L435C, cross-linked products were observed by coincubation with M2M harboring a spacer arm 5.2 Å in length. In contrast, other double-Cys mt PS1 required longer cross-linkers (i.e., M8M with spacer arm of 13.0 Å in M84C/I387C, V89C/I387C, and V94C/L383C; M11M with spacer arm of 16.9 Å in M84C/L435C). Thus, M84 and V89 are predicted to be located in close proximity to the catalytic center, as L383 is located in only two amino acids away from D385, the latter being one of the catalytic aspartates of PS1. These results suggest that the N-terminal region of TMD1 participates in the formation of the hydrophilic structure that resides within the cytosolic side of the catalytic pore.

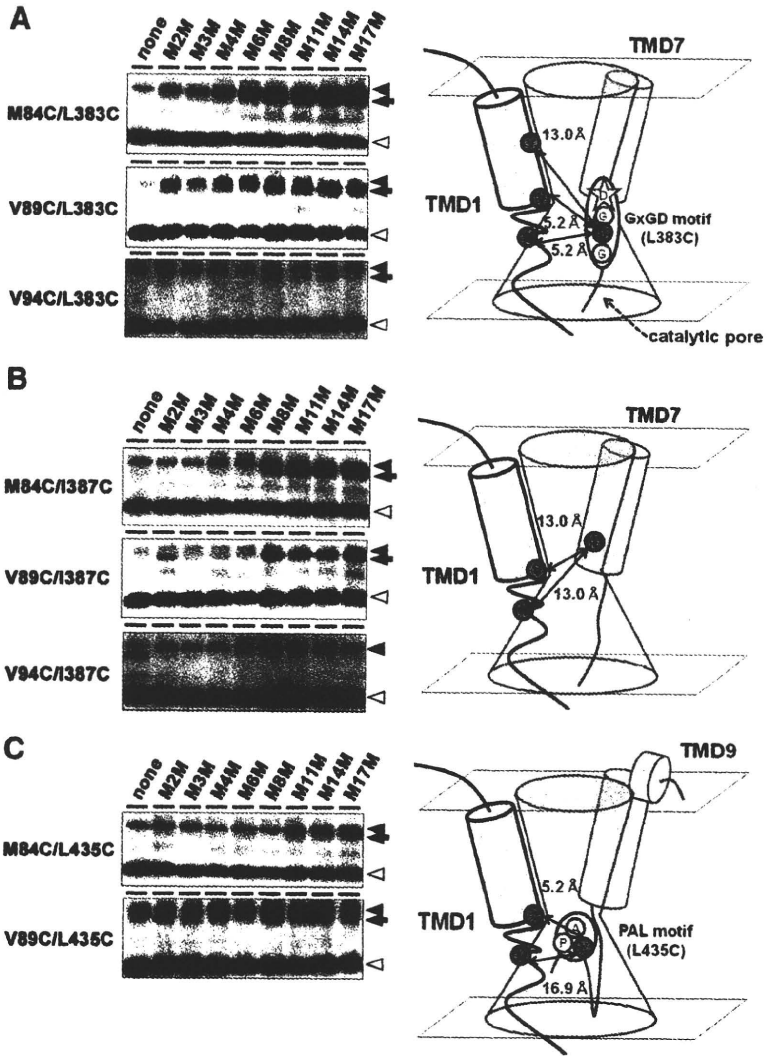

Figure 4. Cross-linking experiments of TMD1 and C-terminal residues using MTS cross-linkers. ***A–C***, Microsome fractions from DKO cells expressing the double-Cys mt carrying one Cys residue at TMD1 and the other at L383C (***A***), I387C (***B***), or L435C (***C***) were incubated with MTS cross-linkers and were separated in SDS-PAGE under nonreducing conditions. Immunoblot analysis was performed using anti-$PS1_{NT}$ antibody. Locations of Cys substitution are shown at the left side of the panel. PS1 FL, NTF, and cross-linked product (NTF-CTF heterodimer) are shown by black arrowheads, white arrowheads, and black arrows, respectively. The predicted maximum lengths between the two residues are indicated in the schematic illustrations at the right side.

Effects of γ-secretase inhibitors on the MTS labeling of TMD1 and Aβ secretion

Next, we examined the effects of three GSIs (i.e., L-685,458, pep15, and DAPT) that have been well characterized functionally and belong to distinct classes of inhibitors on the accessibility of MTSEA-biotin to substituted Cys residues as previously described (Sato et al., 2006, 2008). L-685,458 is a transition-state analog-type GSI that targets the catalytic aspartates, and directly binds NTF and CTF of PS1 (Li et al., 2000; Shearman et al., 2000). Pep15 is a helical peptide-based GSI mimicking the TMD structure, which also binds to PS1 NTF and CTF but does not share the binding site with the transition-state analog inhibitors (Das et al.,

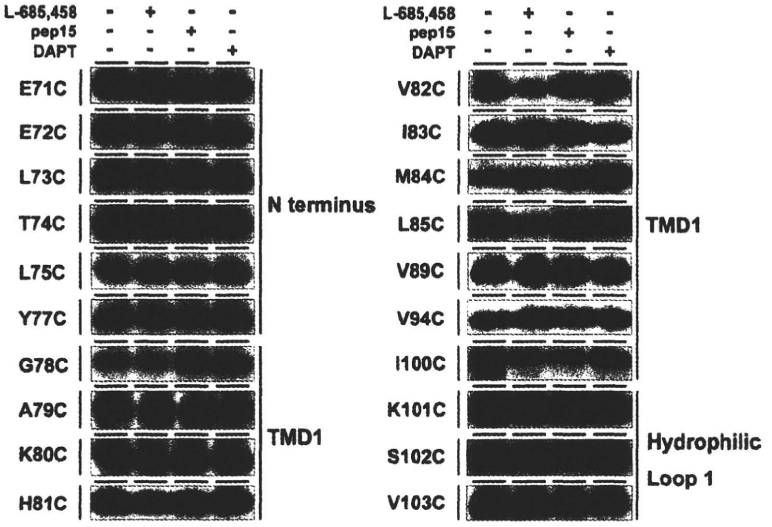

Figure 5. Labeling competition by γ-secretase inhibitors. Biotin labeling of single-Cys mt PS1 was performed after preincubation with L-685,458, pep15, or DAPT. Locations and predicted topology of Cys mutations are shown at left and right, respectively.

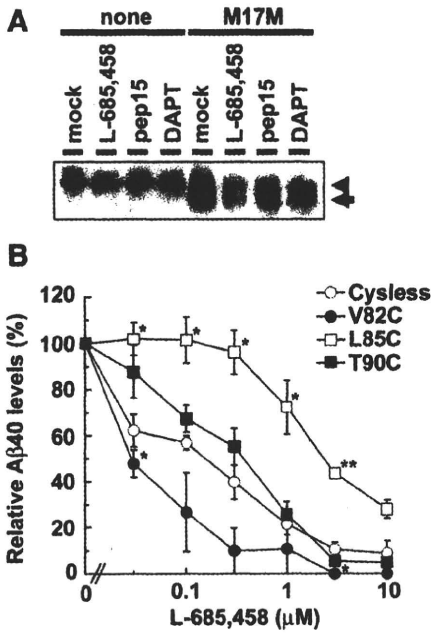

Figure 6. Effect of γ-secretase inhibitors on cross-linking and γ-secretase activity in Cys mt PS1. ***A***, Cross-linking experiment on PS1 harboring double Cys (M84C and I387C) was performed in the presence of L-685,458, pep15 or DAPT. Immunoblot analysis was performed using anti-$PS1_{NT}$ antibody. PS1 FL and cross-linked product (NTF-CTF heterodimer) are shown by black arrowheads and black arrows, respectively. ***B***, Inhibitory effect of L-685,458 on the Aβ40 secretion from DKO cells expressing PS1/Cys(−), V82C, L85C, or T90C. Secreted Aβ40 in conditioned media was quantitated by ELISA [$n = 3$; mean ± SE; $^{*}p < 0.05$, $^{**}p < 0.01$ compared with PS1/Cys(−)].

2003; Kornilova et al., 2005). A dipeptidic inhibitor, DAPT binds to PS1 CTF at a site distinct from, but overlapping with, those of transition-state analogs and helical peptides (Kornilova et al., 2003, 2005; Morohashi et al., 2006). Surprisingly, all three GSIs augmented the labeling of G78C, suggesting that the water accessibility of G78 is increased in an enzymatically inactive γ-secretase. In sharp contrast, the labeling of I100C was decreased by preincubation with one or the other of GSIs. The reciprocal changes in the water accessibility of G78 and I100, which are presumed to be located at the cytoplasmic and luminal borders of TMD1, respectively, upon incubation with the GSIs, may implicate a vertical movement of TMD1 depending on the enzymatically active or inactive states of PS1. In addition, the accessibility of MTSEA-biotin to V82C and L85C was substantially decreased specifically with L-685,458 (Fig. 5), similarly to A246C, L381C, and Cys mutants around the PAL motif (Sato et al., 2006, 2008). Together with the data from cross-linking experiments, these results suggest that L-685,458 occupies the hydrophilic space formed by TMDs 1, 7, and 9 at the cytosolic side of the pore, and that V82 and L85 are involved in the binding of L-685,458. To further test this possibility, we examined the effects of GSIs on the cross-linking of M84C/I387C. The biotinylation of I387C single Cys mutant PS1 was not affected by preincubation of GSIs, as in M84C single Cys mutant (Fig. 5) (Sato et al., 2006). However, the amount of cross-linked products in M84C/I387C was significantly decreased by preincubation with L-685,458 (Fig. 6*A*). We have shown that L-685,458, which targets the catalytic site as well as the subsites of γ-secretase (Li et al., 2000), specifically affected the labeling of residues near these cross-linked residues [i.e., V82 and L85 (Fig. 5); L381 and L383 (Sato et al., 2006)]. Thus, the binding of L-685,458 might sterically interrupt the accessibility of MTS cross-linker to PS1 by occupation of the hydrophilic pore, of which the cytosolic side of TMD1 is involved in its formation. Interestingly, preincubation by DAPT or pep15 also substantially decreased the levels of cross-linked products. The binding sites of these GSIs are overlapped, but different, from those of the transition-state analog (Das et al., 2003; Kornilova et al., 2003, 2005; Morohashi et al., 2006), and the biotinylation of the residues in TMD1 was not affected by either DAPT or pep15. Collectively, these data support the notion that DAPT and pep15 harbor the allosteric effects on the TMD1. Finally, we examined the inhibitory potency of L-685,458 against Cys mutant of TMD1. The inhibitory potency of L-685,458 in DKO cells expressing V82C was significantly augmented, whereas that in L85C was decreased, compared with that in PS1/Cys(−). In contrast, T90C, which was not labeled by MTSEA-biotin, showed a similar response to L-685,458 compared with PS1/Cys(−) (Fig. 6*B*), suggesting that the amino acid substitution at V82 or L85 significantly altered the structure of the binding site for L-685,458. Collectively, these observations suggest that V82 and L85 at the N-terminal region of TMD1 comprise a part of the subsite for γ-secretase within the catalytic pore.

Discussion

The structure of TMD1 of PS1 in an enzymatically active γ-secretase complex

Here, we show for the first time that TMD1 of PS1, composed of residues G78 to I100, is located in proximity to TMD7 and TMD9, and faces the catalytic pore of γ-secretase within the lipid bilayer (Fig. 7*A*). Amino acid alignment of PS orthologs reveals that most of the PS family members harbor a highly conserved proline–valine (PV) residues (at 88th and 89th positions in human PS1) at the center of the putative TMD1 (supplemental Fig.

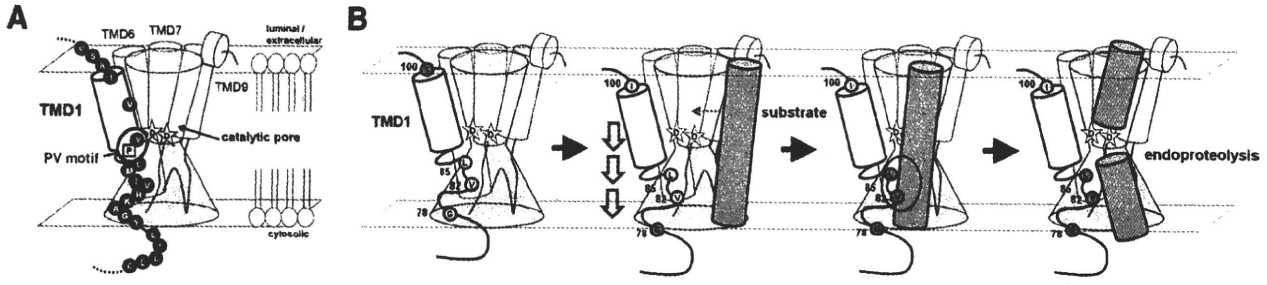

Figure 7. Structure and function of TMD1 of PS1 in relation to the γ-cleavage. ***A***, Summary of SCAM analysis and a schematic depiction of the configuration of the TMD1 in relevance to the catalytic pore. Proline 88 is indicated by a square. Cys mutants that were labeled by MTSEA-biotin are shown in circle frames. Residues whose labeling was competed for by MTS-TEAE, MTSES, and MTSET are shown by blue circles. Residues whose labeling was competed for by MTSES or MTSET, but not by MTS-TEAE, are indicated by sky-blue circles. Residues whose labeling was not affected by any charged residues are indicated by purple circles. ***B***, Schematic presentation of the functional role of TMD1 in the γ-cleavage process. Binding of the substrate to the initial substrate binding site causes the piston movement (purple arrows) and changes the microenvironment of G78 and I100 at the membrane border (indicated by gray and blue circles as decreased and increased hydrophilicity, respectively). A substrate is recognized by the subsite in the catalytic pore (purple oval) where V82 and L85 at N-terminal region of TMD1 (orange circles) are involved in its formation.

6, available at www.jneurosci.org as supplemental material). We showed that V89C was accessible to MTSEA-biotin from the cytosolic side, and cross-linkable to residues of the catalytic GxGD and PAL motifs, suggesting that the PV motif in TMD1 is located in proximity to the catalytic center. Transmembrane helix kinks commonly occur at proline residues (von Heijne, 1991). It has also been suggested that mutations of the N- and C-terminal regions of TMD1 differentially affected the PS endoproteolysis and the γ-secretase activity (Brunkan et al., 2005). Consistently, we showed that N- and C-terminal portions of TMD1 divided by the PV motif exhibit distinct labeling patters by MTS reagent: consecutive residues from G78 to L85 were accessible to MTSEA-biotin, whereas V94C was the only labeled residue in the C-terminal region of TMD1. We speculate that the conserved proline 88 produces a kink in a way to separate TMD1 into two functional regions.

We thoroughly analyzed the hydrophilic environment around TMD1 and found that the cytosolic N-terminal region of the TMD1 may constitute the catalytic structure. Consecutive residues from E71C to Y77C are reactive in microsomes with all charged MTS reagents, including charged bulky MTS-TEAE, indicating that the most N-terminal region of PS1 in a functional state is oriented to the cytosol as previously speculated (Doan et al., 1996). However, the labeling of consecutive residues from G78C to H81C, I83C, and M84C was competed with MTSES or MTSET, but not with MTS-TEAE, suggesting that they lie within a narrower hydrophilic environment. The predicted sizes of the head group of MTSET and MTS-TEAE are 5.8 and 8.0 Å, respectively, possibly reflecting the size of the hydrophilic environment around each modified residue. However, the successive pattern of labeling suggests that this region is not embedded in the lipid bilayer in an α-helical structure. This is highly reminiscent of the pattern of biotinylation of the cytosolic side of TMD7, which we interpreted as a "catalytic plug" structure hung in a hydrophilic pore (Sato et al., 2006). Different competition profile (i.e., competed with MTSES and MTSET in TMD1, but not in TMD7) would reflect the heterogeneity of the hydrophilic milieu within the pore. We speculate that the residues in TMD1 with which MTS-TEAE are unreactive (i.e., G78 to L85) form a hydrophilic structure at the membrane interface of the pore. In addition, M84 was cross-linked to L383 at GxGD motif and L435 at PAL motif. Moreover, the labeling of V82C and L85C was, as in Cys mutants of the GxGD motif, specifically decreased by preincubation with L-685,458 (Fig. 5), and these mutants exhibited an altered sensitivity to L-685,458 (Fig. 6*B*). These data suggest that these residues play a critical role in the γ-secretase activity as a subsite that is involved in substrate recognition during endoproteolysis, although an allosteric effect of L-685,458 on the biotinylation cannot be fully excluded. Collectively, these data support the notion that the cytosolic regions of TMDs 1, 7, and 9 are located in close proximity to each other and may cooperatively function as the catalytic plug.

In contrast to the N-terminal half, most residues in the C-terminal half of TMD1 were hydrophobic: only V94 was water accessible with restrictions and cross-linked with L383. However, no GSIs affected the water accessibility of V94C, suggesting that V94 directly faces the catalytic pore as a part of the pore wall, but do not participate in the formation of a subsite. Notably, the Cys substitution of V96, located at the opposite side of V94 in an α-helical model, caused a loss of protein expression. Consistently, TMD1 is involved in the stabilization of the γ-secretase after the complex assembly is completed (Brunkan et al., 2005; Watanabe et al., 2010). Moreover, amino acid alignment also revealed that V96 is highly conserved from plants to mammals (supplemental Fig. 6, available at www.jneurosci.org as supplemental material). Thus, we speculate that the C-terminal region of TMD1 is an essential domain for maintaining the integrity of PS1 structure via hydrophobic interactions with other TMDs. The observation that C92 in TMD1 was cross-linked with C410 or C419 in TMD8, the latter being totally embedded within the lipid bilayer (Sato et al., 2008), by oxidation-mediated cross-linking (Kornilova et al., 2006), supports this view.

We further characterized the unique feature of the catalytic pore in γ-secretase that has not been observed in other I-CLiPs. We previously reported that the extracellularly accessible L250 in TMD6 was cross-linkable with L435 at the PAL motif that is accessible only from the cytosolic side (Sato et al., 2008). In this study, again, MTS cross-linkers were able to connect the residues accessible only from the cytosol with those from the extracellular/luminal side (i.e., M84C/I387C, V89C/I387C, and V94C/L383C) (Fig. 4). These data indicate that the catalytic pore has a connected structure through the cytosolic and extracellular/luminal sides, as suggested by the single particle analysis of the purified enzyme (Lazarov et al., 2006; Ogura et al., 2006; Osenkowski et al., 2009). This is a unique feature specific to γ-secretase/PS, since the resolved structures of other I-CLiPs (i.e., rhomboid and S2P) exhibit water-including crevasses facing only the extracellular or the cytosolic sides, respectively (Urban and Shi, 2008). The γ-secretase cleaves its substrates at multiple sites with a low sequence specificity (Qi-Takahara et al., 2005; Hemming et al.,